Journal of Energy Storage 55 (2022) 105634

Contents lists available at ScienceDirect

Journal of Energy Storage

journal homepage: www.elsevier.com/locate/est

Review Article

Aging aware operation of lithium-ion battery energy storage systems: A review

Nils Collath [a,*], Benedikt Tepe [a], Stefan Englberger [a], Andreas Jossen [a], Holger Hesse [a,b]

[a] Technical University of Munich, TUM School of Engineering and Design, Department of Energy and Process Engineering, Institute for Electrical Energy Storage Technology, Arcisstr. 21, 80333 Munich, Germany

[b] Kempten University of Applied Sciences, Bahnhofstr. 61, 87435 Kempten, Germany

ARTICLE INFO

Dataset link: https://doi.org/10.14459/2022mp1652796

Keywords:
Battery energy storage system
Lithium-ion
Degradation model
Aging
Operation
Optimization

ABSTRACT

The amount of deployed battery energy storage systems (BESS) has been increasing steadily in recent years. For newly commissioned systems, lithium-ion batteries have emerged as the most frequently used technology due to their decreasing cost, high efficiency, and high cycle life. As a result of a multitude of cell internal aging mechanisms, lithium-ion batteries are subject to degradation. The effects of degradation, in particular decreasing capacity, increasing resistance, and safety implications, can have significant impact on the economics of a BESS. Influenced by aging stress factors such as the state of charge, charge–discharge rate, cycle count, and temperature, the extent of degradation is directly affected by the operating conditions. Significant amount of literature can be found that focuses on aging aware operation of BESSs. In this review, we provide an overview of relevant aging mechanisms as well as degradation modeling approaches, and deduce the key aspects from the state of the art in those topics for BESS operation. Following that, we review and categorize methods that aim to increase BESS lifetime by accounting for battery degradation effects in the operation strategy. The literature shows that using empirical or semi-empirical degradation models as well as the exact solution approach of mixed integer linear programming are particularly common for that purpose, as is the method of defining aging costs for the objective function. Furthermore, through a simulation case study, we identify the most relevant stress factors that influence degradation for the key applications of self consumption increase, peak shaving, and frequency containment reserve.

1. Introduction

The installed capacity of BESSs has been increasing steadily over the last years. These systems are used for a variety of stationary applications that are commonly categorized by their location in the electricity grid into behind-the-meter, front-of-the-meter, and off-grid applications [1,2]. In behind-the-meter applications such as peak shaving or as home storage systems, BESSs provide cost savings for the electricity consumer. For front-of-the-meter applications, like energy arbitrage or balancing power provision, revenue generation in the respective energy and power markets is the primary motive for installation of a BESS. Lastly, in off-grid/microgrid applications, BESSs combined with renewable energy sources can be a cost competitive option over solely relying on diesel generators [1]. For the year of 2020, the International Energy Agency estimated the globally installed power of BESSs to 17 GW [3]. While estimates and forecasts for the currently installed capacity and future growth vary, the agreed upon trajectory in the vast majority of reports and studies is strongly upwards [4–6]. This growth in battery energy storage systems is fueled by technology advances and cost reductions for lithium-ion cells, which are now the predominant battery technology used for new installations [5,6].

Despite cell cost reductions, batteries remain the primary cost component for BESSs [7]. Due to a multitude of cell internal aging mechanisms, lithium-ion cells are subject to degradation, which manifests itself in capacity loss, cell resistance increase, as well as safety implications. These degradation effects, most notably capacity loss, can have a significant impact on the profitability of a BESS [8,9]. Aging mechanisms for lithium-ion cells have received significant attention in scientific literature, with multiple reviews available on this subject [10–13]. It is well known and validated through cell aging studies that the rate of degradation depends on external stress factors such as the temperature (T), DOC, SOC, and the C_{rate} [14–19].

With the increasing adoption of electric vehicles (EVs), multiple reviews can be found that focus on the effects of battery degradation specifically for EVs [20,21]. Woody et al. compiled guidelines to extend

* Corresponding author.
E-mail address: nils.collath@tum.de (N. Collath).

https://doi.org/10.1016/j.est.2022.105634
Received 23 April 2022; Received in revised form 1 August 2022; Accepted 3 September 2022
Available online 21 September 2022

Abbreviations

BESS	Battery energy storage system
BP	Balancing power
C_{rate}	Charge-discharge rate
DOC	Depth of cycle
DP	Dynamic programming
E	Exact solution approaches
EA	Energy arbitrage
EOL	End-of-life
EV	Electric vehicle
FCR	Frequency containment reserve
FEC	Full equivalent cycle
H	Heuristics
LAM_{NE}	Loss of active material on the negative electrode
LAM_{PE}	Loss of active material on the positive electrode
LFP	Lithium iron phosphate
LLI	Loss of lithium inventory
MH	Meta-heuristics
MILP	Mixed integer linear programming
NCA	Lithium nickel cobalt aluminum oxide
NLP	Nonlinear programming
NMC	Lithium nickel manganese cobalt oxide
PS	Peak shaving
PSO	Particle swarm optimization
PV	Photovoltaic
RI	Resistance increase
SCI	Self consumption increase
SEI	Solid electrolyte interphase
SimSES	Simulation Tool for Stationary Energy Storage Systems
SOC	State of charge
SPM	Single particle model
V2G	vehicle-to-grid

the service life for lithium-ion batteries used in EVs, laptops, power-tools, and cellphones [22]. Compared to these applications, BESSs and their operation have several key differentiating properties with regards to battery degradation:

- The primary objective in most stationary BESS applications is either a form of revenue generation, like it is the case for energy arbitrage or balancing power provision, or cost reduction, such as for peak shaving or home storage systems [23,24]. This provides an incentive to directly account for the costs related to battery degradation in the operation strategy of BESS through appropriate models. For applications such as cellphones or EVs, there tend to be higher availability requirements, caused by consumer needs for telecommunication or motion, respectively [22].
- The cycle life requirements for many stationary applications significantly exceed those of electric vehicles, especially privately used ones: For residential storage systems used for self-consumption increase and large-scale storage systems used for frequency containment reserve, Kucevic et al. identified a yearly number of FECs in the range of 200 to 300 FECs per year, depending on system sizing [25]. In terms of calendar life, large-scale BESSs are typically planned as long-term assets of up to decades, opposed to short lived consumer goods such as cellphones and laptops.

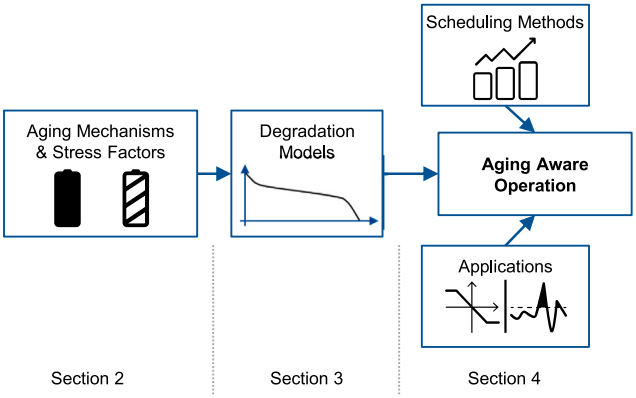

Fig. 1. Schematic overview of this contribution's structure.

- Stationary applications have long been envisioned as a second-life option for decommissioned batteries from EVs [26,27]. While the future economic viability of this concept still remains uncertain today, detailed modeling and mitigation of degradation effects have been described as one of the key areas that require more investigation to enable the profitability of second-life applications [28,29].

Multiple degradation modeling approaches exist to quantify the effects of aging mechanisms and their stress factors [30–32]. These approaches range from data-based empirical models to semi-empirical models with physics-inspired equations, up to detailed physicochemical models, which model individual aging mechanisms through sets of differential equations. All of these bring their own benefits and drawbacks for usage in BESS operation.

A significant number of individual contributions can be found on the topic of BESS operation. The objective commonly is to determine an economically beneficial charge–discharge schedule for one or multiple applications of BESSs. This is done through scheduling methods that can be categorized into exact solution approaches (e.g. mixed-integer linear programming), heuristics (e.g. fuzzy logic) and meta-heuristics (e.g. particle swarm optimization). A review on these methods for BESSs has been published by Weitzel et al. in 2018 [23]. They show that in the contributions published up until then, battery degradation is often either neglected or simplified with constant factors. 25 out of the 202 reviewed studies therein include degradation models [23]. However, especially in more recent years, a number of contributions have integrated more detailed degradation models into scheduling methods [33–38]. Applications of BESSs often overlap with those envisioned for V2G and therefore employ similar scheduling methods. In the field of V2G, Yang et al. reviewed scheduling methods with no particular focus on battery degradation [39]. Ahmadian et al. reviewed degradation models for V2G applications without investigating scheduling methods [32]. An overview of related reviews in the field of aging mechanisms, degradation modeling, and battery operation can be found in Table 1.

In this comprehensive review, we bridge the gap between aging mechanisms, their stress factors and degradation models on the one side, as well as aging aware BESS operation on the other side. We do so by deducing the key aspects for BESS operation from the state of the art in aging mechanisms and degradation modeling (cf. Fig. 1). We start by providing an overview of relevant aging mechanisms and their stress factors for the most commonly used cell types for stationary applications in Section 2. Following that, Section 3 focuses on relevant degradation model types from literature. At the end of both Sections 2 and 3, we deduce the key takeaways of aging mechanisms, stress factors and degradation models for BESS operation. Section 4 categorizes methods for internalizing degradation effects into operation strategies

Table 1
Selected reviews in the field of lithium-ion aging mechanisms, degradation modeling and battery operation.

Topic	Reference	Focus
Aging mechanisms	Edge et al. (2021) [10]	Aging mechanisms in lithium-ion cells
	Han et al. (2019) [20]	Aging mechanisms in automotive lithium-ion battery systems
	Vetter et al. (2005) [12]	Aging mechanisms in lithium-ion cells
Degradation modeling	Li et al. (2019) [30]	State of Health estimation and prediction
	Reniers et al. (2019) [31]	Physicochemical degradation models
	Ahmadian et al. (2018) [32]	Degradation models for V2G applications
	Pelletier et al. (2017) [21]	Degradation models for EVs
Battery operation	Woody et al. (2020) [22]	Strategies to limit battery degradation
	Weitzel et al. (2018) [23]	Scheduling methods for BESSs
	Yang et al. (2015) [39]	Scheduling methods for V2G

based on a comprehensive review of existing literature. In addition, we reveal the most relevant stress factors to consider for key BESS applications through a simulation case study.

2. Aging mechanisms and stress factors

This section provides an overview of the predominant aging mechanisms and their stress factors for commonly used lithium-ion batteries in BESSs.

2.1. Aging mechanisms

Lithium-ion batteries are composed of multiple layers of material wound up or stacked into a cell enclosure [40]. The electrolyte-filled, layered structure of a typical lithium-ion battery consists of: current collectors, the anode and cathode active material, and a separator. Both performance and degradation behavior are strongly influenced by the composition of the anode active material, the cathode active material, the electrolyte, and the resulting interactions of those materials [11,12,20].

Aging mechanisms are commonly grouped into the following four aging modes, based on their effect on the cell: loss of lithium inventory (LLI), loss of active material on the positive electrode (LAM_{PE}), loss of active material on the negative electrode (LAM_{NE}), and resistance increase (RI). LLI describes the loss of lithium ions through parasitic reactions, which can lead to a reduction of the available cell capacity [10,20,41]. LAM_{PE} or LAM_{NE} refer to active material being no longer available for the insertion of lithium on the cathode or anode, respectively [10,20,41]. These aging modes lead to both capacity and power fade. RI refers to aging mechanisms that cause an increase of the cell resistance or impedance and thereby lead to a decrease of the available power [10,20]. Notably, RI also leads to a reduction in usable capacity if the charge and discharge cut-off voltage stay constant [20]. Some authors propose further modes to summarize the effects of aging mechanisms, such as loss of electrolyte [20] and stoichiometric drift [10].

In the following, we confine ourselves to provide a short overview of the most predominant aging mechanisms, as illustrated in Fig. 2, and their effect on the most commonly referenced aging modes: LLI, LAM_{PE}, LAM_{NE}, and RI. Furthermore, we focus on three common cell types. That is, battery cells with graphite-based anodes and one of the following cathode active materials: lithium nickel manganese cobalt oxide (NMC), lithium nickel cobalt aluminum oxide (NCA) or lithium iron phosphate (LFP).

2.1.1. Anode aging mechanisms

Growth of the solid electrolyte interphase (SEI) on the anode surface has been identified as a key aging mechanism for capacity and power fade [10,12]. Graphite from the anode will react with electrolyte and lithium to form this solid passivation layer [12]. The SEI is initially formed within the first few cycles, usually during cell formation by the manufacturer [20]. The resulting passivation layer is aimed to be ionically conducting and electrically insulting [42]. It thereby should allow Li ions to pass through it, while protecting the anode from co-intercalation of solvent molecules and further decomposition of the electrolyte [42]. However, the SEI will continue to grow over a cell's life cycle [13,20]. Solvent molecules may still diffuse through existing SEI, volume change during cycling can lead to cracking and expose additional anode surface area for SEI growth, and side reaction products such as dissolved transition metals from the cathode or plated lithium can form additional SEI [10]. This continued growth of the SEI leads to the aging modes of both LLI and RI [10,20].

Volume change during cycling, solvent co-intercalation, or gas evolution inside the graphite can lead to particle cracking & graphite exfoliation [12]. This in turn can lead to electric contact loss of the active material and thereby induce LAM_{NE} [10,20]. If the anode material loses contact while being lithiated, the lithium will be trapped in the material which induces LLI in addition to LAM_{NE} [10]. Furthermore, additional SEI can form on the newly exposed anode surface area [10].

Lithium plating is a side reaction in which metallic lithium forms on the anode surface instead of intercalating into it [10,12]. This can especially occur through overcharging the cell or while charging at high currents or low temperatures [10,12]. During rest periods and through discharging the reaction is partially reversible, which is referred to as lithium stripping [43,44]. On the other hand, part of the metallic lithium may be enclosed by newly formed SEI, resulting in irreversible LLI [43]. Notably, dendrite growth as a consequence of lithium plating is a significant safety concern, as the dendrites can pierce the separator, short circuit the cell, and induce thermal runaway [45].

Further aging mechanisms on the anode, which are not discussed in detail here, include decomposition of the binder, as well as current collector corrosion [41,46].

2.1.2. Cathode aging mechanisms

Aging mechanisms on the cathode are highly dependent on the cathode material [10]. For most metal oxides, the predominant mechanisms on the cathode side are particle cracking, structural decomposition, transition metal dissolution, and formation of the cathode electrolyte interface [20,47].

Same as the anode, the cathode material is subject to volume change during charge and discharge, which can lead to particle cracking and thereby induce LAM_{PE} [10,41]. Also, if the cathode active material loses contact while being lithiated, this will lead to LLI in addition to LAM_{PE} due to trapped lithium [10]. Structural disordering describes a reaction in which Li^+ ions exchange spots with transition metal ions inside the lattice, which can induce LAM_{PE} and RI [10,12,20]. Similar to the SEI, a cathode electrolyte interface forms through reaction of the cathode with the electrolyte. While this passivation layer is usually thinner than the SEI, it nevertheless induces RI and LAM_{PE} [10,20]. Lastly, transition metal dissolution from the cathode into the electrolyte can lead to LAM_{PE} as well [20,30]. The dissolved metal is known to then move to the anode and further accelerate SEI growth there [12].

Further reported degradation mechanisms on the cathode include electrolyte decomposition and loss, phase change to the lattice, binder decomposition, and current collector corrosion [10,46].

For NMC cathodes, transition metal dissolution and structural disordering have been reported as a prime concern due to the similar radii

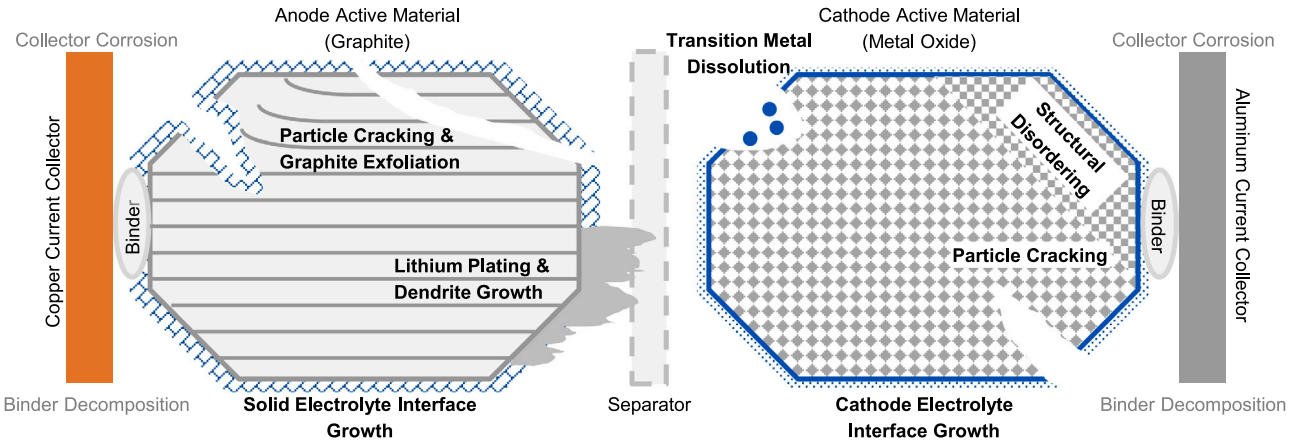

Fig. 2. Schematic illustration of predominant aging mechanisms in common lithium-ion batteries with graphite based anodes and metal oxide cathodes, based on [10,12,41].

of Li^+ and Ni^{2-} [12,48]. The degradation behavior of NMC cathodes is also influenced by their stoichiometry. To both increase energy density and reduce cobalt usage, NMC materials with higher nickel content, such as (NMC)-811, are receiving increased attention. This increase of Ni in the cathode mix shows disadvantageous effects on cycle stability, due to among other the before-mentioned cation mixing of Li^+ and Ni^{2-} as well as increased microcrack formation of (NMC)-811 compared to for example (NMC)-111 [11]. For lithium nickel cobalt aluminum oxide (NCA) cathodes, particle cracking has been reported as a main concern for cycle stability [48]. While cycle life also depends on cell design and cycle conditions, commercial LFP cells tend to show higher cycle stability than their NMC and NCA counterparts [49].

2.2. Aging stress factors

The aging behavior of lithium-ion cells is influenced by a multitude of factors. In the following, we will examine those external stress factors that can be influenced through appropriate operation strategies for BESSs. It should be noted that production quality and cell design parameters, such as the electrode thickness and choice of electrolyte additives, have a significant effect on the aging behavior of lithium-ion cells as well [20], but cannot be influenced in the operation phase of a BESS. Furthermore, extreme stress conditions outside of standard operating conditions can lead to catastrophic failure and thermal runaway, such as high temperature, high charge–discharge rates as well as overcharge and over-discharge of cells [50,51]. Such operating conditions should be prevented by appropriate design and battery management systems.

While the effects of aging mechanisms are commonly grouped into the four previously introduced aging modes (i.e. LLI, LAM_{PE}, LAM_{NE}, RI), a useful framework for BESS operation is the concept of calendar and cyclic aging, as depicted in Fig. 3. Cyclic aging refers to degradation effects that occur as a consequence of cycling the battery, i.e. charging and discharging. Calendar aging describes aging effects that occur regardless of cycling and especially during storage or idle time.

2.2.1. Calendar aging

Calendar aging is primarily influenced by time, temperature and the state of charge of the battery cells:

Time t: While not directly controllable during operation, side reactions such as SEI growth and binder decomposition will progress over time even without cycling the battery.

Temperature T: During storage, a higher temperature will lead to a higher reaction rate of the relevant side reactions, especially SEI growth, and therefore accelerate cell degradation [12].

State of Charge SOC: A high SOC comes with a low anode and high cathode potential. The low anode potential is known to accelerate SEI

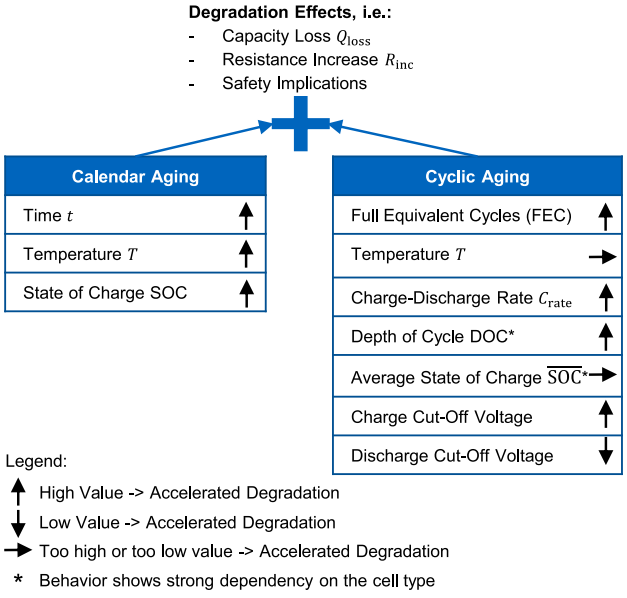

Fig. 3. Relevant stress factors during operation of a BESS and their effect.

growth, therefore a high SOC will accelerate cell degradation [12,20]. Likewise, the high cathode potential can lead to increased transition metal dissolution due to oxidation of the lattice oxygen in NMC cathodes [10]. A calendar aging study conducted by Keil et al. with commercial NMC, NCA and LFP cells, all with graphite anodes, showed the lowest capacity loss for those cells that were stored at 0% SOC for all three cathode materials [52]. Instead of the normalized SOC, the cell terminal voltage V_{cell} may sometimes be used as an equivalent stress factor in degradation models [15]. For extended storage times, a direct relation from SOC to V_{cell} is given through the open circuit voltage curve.

2.2.2. Cyclic aging

Multiple stress factors impact the extent of cyclic aging: Next to temperature, the cycling parameters charge–discharge rate C_{rate}, average state of charge $\overline{SOC}$, and depth of cycle DOC determine the extent of cyclic aging. These cycling parameters are illustrated in Fig. 4. Furthermore, the operating voltage window, determined by the charge and discharge cut-off voltage have known impact on cyclic aging.

Full Equivalent Cycles FEC: The majority of aging mechanisms are either directly caused or accelerated by charging and discharging the

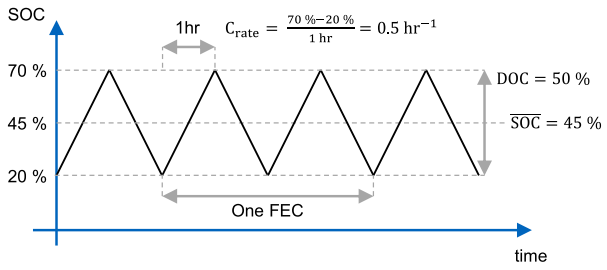

Fig. 4. Visualization of normalized battery cell cycling parameters: Here, an exemplary cell is cycled at a depth of cycle DOC of 50% around an average state of charge $\overline{SOC}$ of 45% at a charge–discharge rate C_{rate} of 0.5 h^{-1}. A total of two full equivalent cycles FECs are displayed.

cell: particle cracking & graphite exfoliation, lithium plating & dendrite growth, structural decomposition, transition metal dissolution, as well as additional SEI growth induced by the aforementioned mechanisms. The amount of cycling is commonly stated in full equivalent cycles (FECs), by scaling the total charge throughput Q with the battery capacity C_{batt} in Ah:

$$Q = \int_0^t |I(t')|\, dt' \tag{1}$$

$$\mathrm{FEC} = \frac{Q}{2 * C_{batt}} \tag{2}$$

Here, I is the charge–discharge current. For C_{batt}, multiple definitions exist, as either the nominal battery capacity at the beginning of life or the present, degraded battery capacity may be used.

Temperature T: Especially while charging, low temperatures can lead to lithium plating on the graphite anode and thereby accelerate degradation [12,53]. On the other hand, the additional SEI growth caused by volume expansion, particle cracking and graphite exfoliation, as well as transition metal dissolution are further accelerated when cycling at high temperatures [53,54]. With low temperatures causing lithium plating and high temperatures accelerating SEI growth and transition metal dissolution, the temperature of a lithium-ion based BESS should ideally be neither too high nor too low [53,54]. It should be noted that a low operating temperature also negatively affects the available cell capacity as well as the cell resistance and thereby energetic efficiency. A range of 15 to 35 °C is often stated for the optimal operating temperature of lithium-ion cells [55].

Charge-Discharge Rate C_{rate}: To normalize for the battery capacity C_{batt}, the charge–discharge rate C_{rate} in h^{-1} is often given instead of the charge–discharge current I:

$$C_{rate} = \frac{I}{C_{batt}} \tag{3}$$

A high C_{rate} will accelerate particle cracking & graphite exfoliation as well as additional SEI formation [10,56]. Charging and discharging a cell for the same amount of FECs, but with a higher C_{rate}, can therefore accelerate capacity loss and resistance increase, as it was shown in a cyclic aging study by Naumann et al. with LFP-graphite cells [19]. It should be noted that a high C_{rate} will also cause the cell to generate more heat and increase its temperature, making it challenging to distinctly separate individual stress factors. In a study conducted by Barcellona et al. cells were kept in a temperature range of 20 to 30 °C through active cooling with Peltier cells [57]. For the investigated lithium cobalt oxide cells with graphite anodes, the impact of the C_{rate} on capacity loss was found to be negligible for moderate charge–discharge rates [57]. Especially in combination with low temperatures or at a high SOC, lithium plating & dendrite formation on the anode may occur when charging with a high C_{rate} [12]. Fast charging with a high C_{rate} is especially required for EV and consumer electronic applications. During fast charging, the combination of inhomogeneous temperature distribution in the cell, lithium plating risk, and mechanical stress is the main concern for cell aging [58]. Notably though, typical stationary BESS applications require a lower C_{rate} in both charge and discharge direction [25].

Average State of Charge $\overline{SOC}$: The average state of charge $\overline{SOC}$ around which a cell is cycled is known to influence cyclic aging as well. In an aging study by Schmalstieg et al. NMC-graphite cells were cycled with a fixed DOC of 10% in different SOC ranges. After normalizing for the effects of SOC on calendar aging, the lowest cyclic aging was found in the range of 45 to 55% SOC, at $\overline{SOC}$ = 50%, and the highest in the range of 90 to 100% SOC, at $\overline{SOC}$ = 95%. In an experimental study focusing on this stress factor, Gantenbein et al. attributed the impact of SOC ranges to different stages of lithiation of the graphite anode [59]. The graphite anode will expand in volume when charging and retract when discharging [59,60]. Volume expansion and retraction of the graphite anode is especially pronounced when transitioning between these lithiation stages [60]. Cycling between lithiation stages is therefore expected to cause increased particle fraction and formation of new SEI [59]. The average cell terminal voltage $\overline{V_{cell}}$ may be used to quantify this stress factor in degradation models as well [15].

Depth of Cycle DOC: The DOC is sometimes also referred to as depth of discharge (DOD or ΔDOD) or cycle depth in literature. It refers to the difference in SOC levels between which a cell is cycled, as illustrated in Fig. 4. The general tendency of higher capacity loss with higher DOC has been attributed to increased cracking and new SEI Formation as a consequence of volume expansion in the graphite anode, especially when crossing the anode's phase change regions [59,61]. While in general a higher DOC will increase capacity loss, exceptions are found in empirical aging studies. In a study conducted by Ecker et al. with commercial NMC-graphite cells, the general trend showed a higher capacity loss with increasing DOC, for the same $\overline{SOC}$ and number of FECs [62]. An exception being that after 750 FECs, cycling between 85% and 75%, at DOC = 10%, showed less degradation than between 82.5% and 77.5%, at DOC = 5% [62]. In another aging study with commercial LFP-graphite cells by Naumann et al. higher DOCs lead to higher capacity loss after extended cycling as well [19]. An exception being that for low DOCs, a capacity recovery effect was observed: After an initial accelerated capacity loss for lower DOCs such as 10% and 20% compared to higher DOCs of 80% and 100%, part of that capacity loss for low DOCs is regained following further cycling [19]. This effect was later attributed to non-uniform lithium distribution after extended shallow cycling at low DOC [63].

Charge and Discharge Cut-Off Voltage: The usable and nominal capacity and thereby the definition of the SOC are dependent on the set operating voltage limits of a cell, i.e. the charge and discharge cut-off voltage. A high charge cut-off voltage can lead to over-delithiation of the cathode material and thereby accelerate structural disordering on the cathode [30]. Furthermore, over-lithiation of the anode can lead to lithium plating and dendrite formation [12]. Low discharge cut-off voltages can lead to corrosion of the anode's copper current collector [30]. The operating voltage window should therefore be set such that the cells deliver a high nominal capacity while retaining high cycle life. Juarez-Robles et al. observed more than double the cycle life at a 20% reduction in usable capacity by limiting the manufacturer's recommended safe discharge and charge cut-off voltage from [2.7 V, 4.2 V] to [2.9 V, 4.0 V] for a commercial NCA-graphite cell [64]. In a similar setup of commercial cells with NCA cathodes and graphite/silicon composite anodes, Bazlen et al. found that by decreasing the charge cut-off voltage from 4.2 V to 4.1 V cathode aging effects can be reduced [65]. Increasing the discharge cut-off voltage from 2.5 V to 3.1 V, reduced anode aging, which was attributed to less volume change of the graphite/silicon anode [65].

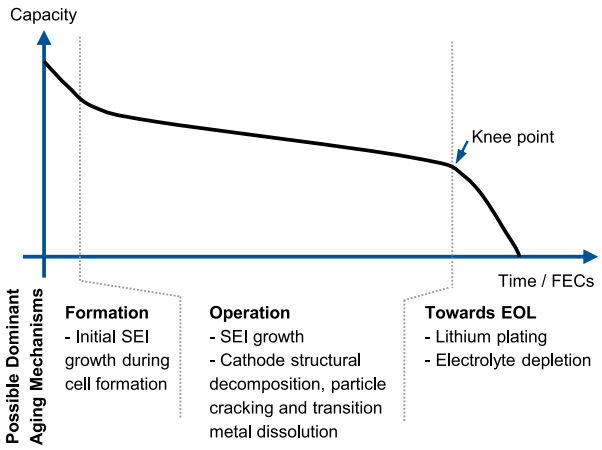

Fig. 5. Schematic depiction of capacity loss and possible dominant aging mechanisms over a cell's life cycle for graphite anodes and metal oxide cathodes. Based on [20,66].

2.3. Key aspects of aging mechanisms and stress factors for BESS operation

The previous sections provided an overview of the relevant aging mechanisms and their stress factors in common lithium-ion batteries with graphite based anodes and metal oxide cathodes. The specific degradation behavior is dependent on cell design, electrolyte additives and the cathode material, but the primary aging mechanisms and their stress factors remain the same across LFP, NMC and NCA.

Past studies have shown that over a cell's life cycle the dominant aging mechanisms vary as highlighted in Fig. 5. The initial formation of the SEI is mostly completed during production as one of the costliest manufacturing steps [67,68]. During the main operation phase, degradation for standard operating conditions is to a large extent driven by SEI growth combined with the cathode aging mechanisms [20,69,70]. Once the SEI has grown extensively, a self-reinforcing process of lithium plating may lead to rapid capacity loss [69,70]. The SEI growth leads to a reduction of the anode's ionic kinetics that can induce lithium plating even during standard operating conditions. If the plated lithium is isolated by formation of additional SEI around the lithium, this will lead to further deterioration of the anode's ionic kinetics and in turn promote further lithium plating [69,70]. Extensive loss of non-lithiated anode active material can also induce lithium plating and thereby rapid capacity loss. This is due to over-lithiation of the anode during charging, as the remaining anode active material may be unable to accommodate all remaining lithium [71]. Electrolyte depletion has been reported to cause significant loss of active material and thereby rapid capacity loss as well after extended operation [66,72]. The onset of this phase of rapid degradation is often referred to as an aging knee point, with a review of possible mechanisms leading to this knee point having been compiled by Attia et al. [73]. Notably, in a cell aging study by Johnen et al. the phase of rapid capacity loss was followed by another phase of slow degradation for low remaining capacity between 20% and 30% of the initial capacity [74].

Typically, the cell end-of-life (EOL) is defined before this region of rapid degradation between 70% and 80% remaining capacity [74,75]. This range is also commonly found in manufacturer warranties [76]. Instead of a fixed figure for the remaining capacity, application specific profitability criteria have been proposed to determine the EOL for BESSs, which may result in a system being operated up to lower remaining capacity [33,75]. It should be considered though that operating cells with low remaining capacity can negatively affect cell safety, especially in the presence of lithium plating [77–79].

While the specific degradation behavior is cell dependent, general conclusions can be drawn on how to extend BESS lifetime. During idle time, SOC and T should be kept low. During charging and discharging, capacity loss can be reduced by keeping the temperature T in a medium range, by avoiding phase change regions of the anode with $\overline{\mathrm{SOC}}$, and by cycling at low DOC and C_{rate}.

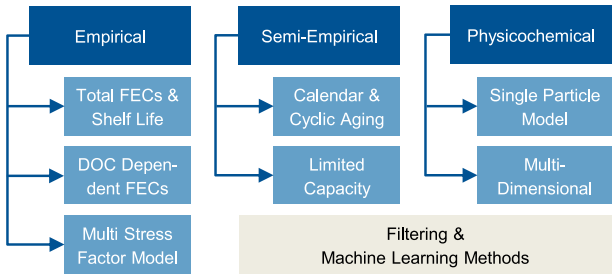

Fig. 6. Classification of degradation models.

3. Degradation models

Degradation models quantify the effects of aging mechanisms as a function of a cell's properties and usage profile. As we will show in Section 4, most publications in the field of BESS operation investigate capacity loss as the primary effect of battery degradation, due to its detrimental effect on the remaining useful life and the profitability of a BESS. We therefore focus on models that describe capacity loss. Depending on a degradation model's use-case, other effects may be relevant as well such as resistance increase to quantify power fade or the extent of cell internal lithium plating to assess safety risks.

3.1. Model types

Degradation models can loosely be categorized into empirical, semi-empirical and physicochemical models with further sub-categorization as shown in Fig. 6.

3.1.1. Empirical models

Empirical models are fit to cell aging data, without inherent modeling of the underlying physical aging mechanisms. Varying degrees of complexity for such models can be found.

The most simple form of an empirical model is the assumption that battery life is limited by a total amount of usable FECs in combination with a shelf life (e.g. 1500 FECs and 10 years). If either the total amount of FECs or shelf life is reached, the battery is assumed to have reached its EOL [80]. Though simple, this model does not account for any of the stress factors from Section 2.2.

DOC dependent total FEC models account for the fact that a small amount of cycles at high DOC tend to cause more battery degradation than the equivalent amount of cycles at a low DOC. This type of model has been employed by multiple authors for BESS operation [80–83].

Multi stress factor empirical models link any number of additional stress factors to capacity loss. For example, Padmanabhan et al. used a model that accounts for both the DOC and C_{rate} dependence of capacity loss [84]. Fig. 7 provides a visualization of a degradation model from Maheshwari et al. with dependence on DOC, $\overline{\mathrm{SOC}}$ and C_{rate} [85].

3.1.2. Semi-empirical models

Semi-empirical models typically rely on data from cell aging studies, in which a limited number of cells has been cycled and stored under accelerated aging conditions. For model fitting, they use functions that describe the underlying aging mechanisms. Multiple frequently used models use a superposition approach of calendar and cyclic loss to describe the total capacity loss, as indicated in Eq. (4) [15–19,54,86,87].

$$Q_{\mathrm{loss}}^{\mathrm{total}} = Q_{\mathrm{loss}}^{\mathrm{cal}}(t, \mathrm{SOC}, T) + Q_{\mathrm{loss}}^{\mathrm{cyc}}(\mathrm{FEC}, C_{\mathrm{rate}}, T, \overline{\mathrm{SOC}}, \mathrm{DOC}) \tag{4}$$

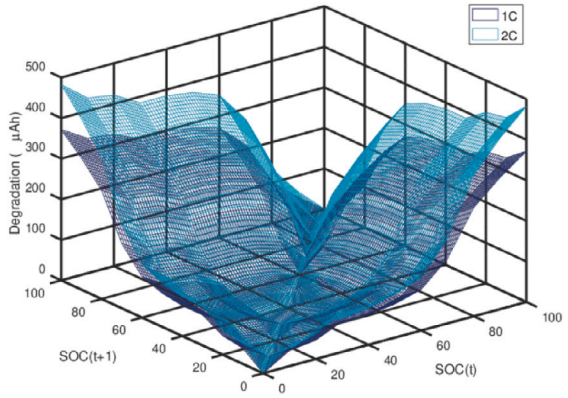

Fig. 7. Multi stress factor empirical model for a NMC cell, as depicted in Maheshwari et al. [85].

Here, $Q_{\text{loss}}^{\text{total}}$ refers to the total capacity loss while $Q_{\text{loss}}^{\text{cal}}$ and $Q_{\text{loss}}^{\text{cyc}}$ refer to the calendar and cyclic components of capacity loss, respectively. Table 2 provides an overview of selected semi-empirical degradation models.

Calendar Aging: For the calendar capacity loss $Q_{\text{loss}}^{\text{cal}}$, the selected models show a degree of uniformity: The common assumption of a square root dependency of $Q_{\text{loss}}^{\text{cal}}$ on time can be traced back to approximating SEI growth as a diffusion limited process for graphite electrodes [56]. More general power law and logarithmic expressions are also used for the time dependency of calendar aging by some authors [15,88]. The Arrhenius equation describes the exponential temperature dependency of reaction rates and is commonly referenced for modeling temperature dependent calendar aging [18,54,89–92]. Eq. (5) shows an adapted version of the Arrhenius equation as it can be used for fitting to aging test data [88,93].

$$\alpha_T = \gamma_1 * e^{-\frac{\gamma_2}{R}*(\frac{1}{T}-\frac{1}{T_{ref}})} \tag{5}$$

α_T refers to the stress factor and γ_1 and γ_2 are fitting parameters, analogously to Table 2. R is the gas constant and T_{ref} the reference temperature for data fitting.

The Tafel equation describes the overpotential of an electrochemical reaction as a function of current density. Under the assumption that SEI growth is driven by over-potential, multiple authors use Tafel-like equations to describe the effect of SOC on calendar aging [54,88,91], see Eq. (6).

$$\alpha_{\text{SOC}} = \gamma_1 * e^{-\frac{\gamma_2 * F}{R} * \frac{U_{\text{a,ref}} - U_a(\text{SOC})}{T_{\text{ref}}}} \tag{6}$$

α_{SOC} is the stress factor, F is Faraday's constant and U_a the anode to reference potential. Simplified exponential expressions of the above dependency of α_{SOC} on SOC are used in the Saraketa-Zabala et al. and Guenther et al. models from Table 2 [16,86].

Cyclic Aging: The highlighted cyclic aging models show notably less uniformity in both model structure and the considered stress factors than the calendar aging models. Generally, cyclic aging models tend to use either cumulative charge throughput Q [15,17,92] or the total number of FECs [19,54,94] to represent battery cycling. On the other hand, the model of Guenther et al. relies on summation after every cycle to account for both the effect of cycling and the DOC of each cycle [86]. While most cyclic aging models tend to consider the DOC dependence, only some include further stress factors. Schmalstieg et al. also accounted for the average cell voltage during cycling V_{cell} [15]. Naumann et al. included the charge–discharge rate C_{rate} dependency in addition to the DOC in their model [19]. While not part of Table 2, Schimpe et al. published a cyclic aging model that also accounts for temperature dependence [54].

Smith et al. took a different approach to semi-empirical degradation modeling [95], labeled **Limited Capacity** in Fig. 6. Their model computes the available remaining capacity as the minimum of lithium inventory limited capacity, negative electrode limited capacity and positive electrode limited capacity. All three components are then described as physics inspired algebraic equations and fitted to aging test data [95].

3.1.3. Physicochemical models

Physicochemical models describe cell internal degradation mechanisms through sets of differential equations. Compared to empirical and semi-empirical models they are often considered computationally expensive, but promise extrapolation outside of the experimental data sets if parameterized accurately [88,96]. Generally, physicochemical models focus on individual degradation mechanisms such as SEI growth or particle cracking [31]. A detailed overview of published physicochemical degradation models and the considered mechanisms for each model has been compiled by Reniers et al. [31].

As a reduced order physicochemical model, single particle models (SPMs) provide a trade-off between computational efficiency and accuracy [97]. Under the assumption of uniform current distribution as well as same size spherical particles in both electrodes, each electrode is approximated as a single, spherical particle [97]. Ning et al. provided a SPM to describe SEI growth at the negative electrode under consideration of external stress factors [98]. At the core of the degradation model, the capacity loss caused by SEI growth is described by the current density of the solvent reduction side reaction, as shown in Eq. (7).

$$\frac{\partial Q_{\text{loss}}^{\text{SEI}}(t)}{\partial t} = i_{\text{s}}(t) * A_{\text{n}} \tag{7}$$

With $Q_{\text{loss}}^{\text{SEI}}$ being the capacity loss caused by SEI growth, i_{s} the side reaction current density and A_{n} the surface area of the negative electrode. Further differential equations then describe the side reaction current density as a function of over-potential in a Tafel-like equation [98]. Other authors use similar SPM formulations with notable examples provided in the following [97,99]. For increased accuracy, Pinson et al. added a one-dimensional porous electrode model to their SPM that accounts for spatial in-homogeneity of the SEI [99]. Li et al. developed a SPM that in addition to SEI growth considers crack propagation due to volume change [97]. Some more complex degradation models build on top of a modeling framework that is often referred to as the pseudo two-dimensional (P2D) Newman model [100,101]. Aswhin et al. proposed an SEI growth model based on the P2D Newman model [102]. Yang et al. developed a model that in addition to SEI growth, accounts for lithium-plating in order to represent the fast, nonlinear capacity loss towards the EOL [70]. Similarly, the model by Keil et al. represents SEI formation, SEI re-formation due to particle cracking, as well as lithium plating and lithium stripping [103].

3.1.4. Filtering and machine learning methods

Filtering and machine learning methods for capacity degradation modeling typically use online data of the system of interest. A review of methods in this field has been compiled by Li et al. [30]. Bayesian filters such as Kalman filters and particle filters allow to estimate and update the fitting parameters of degradation models during the operation phase [30,104]. Machine learning methods, such as artificial neural networks and support vector machines, rely on training data to tune the models before being applied to online data of the system of interest [105,106]. While filtering and machine learning methods are frequently proposed for the online estimation of the state of health [107] or remaining useful life of lithium-ion cells [108,109], none of the investigated publications in the field of BESS scheduling use such methods for degradation modeling. Especially machine learning methods, such as neural networks, tend to not provide a direct algebraic link between external stress factors and capacity loss, which makes them challenging to integrate into scheduling methods.

Table 2
Algebraic form of selected semi-empirical degradation models. α_i and β_i refer to the algebraic form of the calendar and cyclic stress factors, respectively. The index denotes the specific stress factor. γ_i refers to a fitting parameter that is determined based on accelerated cell aging tests in the respective studies.

		Schmalstieg (NMC) [15]	Naumann (LFP) [18,19]	Sarasketa-Zabala (LFP) [16,17]	Guenther (generic cell) [86]
$Q_{\text{loss}}^{\text{cal}}$	=	$\alpha_T * \alpha_{V_{\text{cell}}} * t^{0.75}$	$\alpha_T * \alpha_{\text{SOC}} * t^{0.5}$	$\alpha_T * \alpha_{\text{SOC}} * t^{0.5}$	$\alpha_T * \alpha_{\text{SOC}} * t^{0.5}$
α_T	=	$\gamma_1 * e^{-\frac{\gamma_2}{T}}$	$\gamma_1 * e^{-\gamma_2 * (\frac{1}{T} - \frac{1}{T_{\text{ref}}})}$	$\gamma_1 * e^{-\frac{\gamma_2}{T}}$	$\gamma_1 * e^{\frac{T - T_{\text{ref}}}{\gamma_2}}$
$\alpha_{\text{SOC},V_{\text{cell}}}$	=	$(\gamma_1 * V_{\text{cell}} - \gamma_2)$	$\gamma_1 * (\text{SOC} - 0.5)^3 + \gamma_2$	$\gamma_1 * e^{\gamma_2 * \text{SOC}}$	$e^{\frac{\text{SOC} - \text{SOC}_{\text{ref}}}{\gamma}}$
$Q_{\text{loss}}^{\text{cyc}}$	=	$(\beta_{V_{\text{cell}}} + \beta_{\text{DOC}} + \gamma) * Q^{0.5}$	$\beta_{\text{C-rate}} * \beta_{\text{DOC}} * \text{FEC}^{0.5}$	$\beta_{\text{DOC}} * Q^{\gamma}$	$\sum_{n=0}^{N} \beta_{\text{DOC},n}$
$\beta_{\overline{\text{SOC}},\overline{V_{\text{cell}}}}$	=	$\gamma_1 * (\overline{V_{\text{cell}}} - \gamma_2)^2$	–	–	–
β_{DOC}	=	$\gamma * \text{DOC}$	$\gamma_1 * (\text{DOC} - 0.6)^3 + \gamma_2$	10% ≤ DOC ≤ 50%: $\gamma_1 * \text{DOC}^2 + \gamma_2 * \text{DOC} + \gamma_3$ Else: $\gamma_4 * e^{\gamma_5 * \text{DOC}} + \gamma_6 * e^{\gamma_7 * \text{DOC}}$	$\gamma_1 * \text{DOC}^3 + \gamma_2 * \text{DOC}^2 + \gamma_3 * \text{DOC}$
$\beta_{\text{C-rate}}$	=	–	$\gamma_1 * \text{C}_{\text{rate}} + \gamma_2$	–	–

Table 3
Assessment of different degradation model types for BESS operation.

Model type	Advantages	Disadvantages
Empirical	• high computational efficiency • can include all aging effects represented in the data	• strong reliance on aging data • limited extrapolation capacity
Semi-empirical	• high computational efficiency • minor extrapolation capacity	• strong reliance on aging data
Physicochemical	• high extrapolation capacity for the modeled mechanisms • model provides multiple cell parameters in addition to capacity loss	• high parameterization effort • computationally expensive

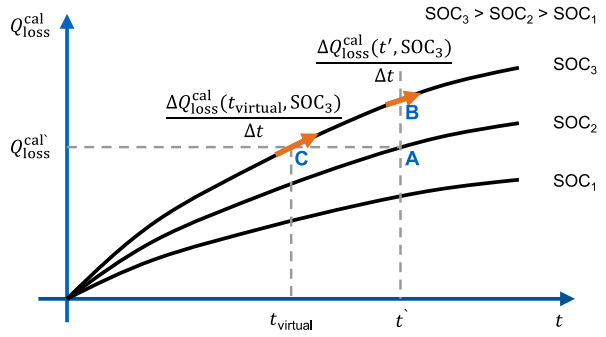

Fig. 8. Qualitative depiction of deriving the virtual time and the related degradation rate for changing from storage SOC_2 to storage SOC_3.

3.2. Key aspects of degradation models for BESS operation

Table 3 summarizes the key advantages and disadvantages of the different degradation model types for BESS operation. Empirical models provide no modeling of the underlying aging mechanisms and therefore solely rely on aging data. Physicochemical models model the underlying mechanisms in detail through sets of differential equation, require less aging test data, but in exchange bring a high parameterization effort with them. If the modeled aging mechanisms do not fundamentally change in the investigated time frame, a certain degree of extrapolation capacity can be assumed outside of the validation period with physicochemical models [88]. Semi-empirical models attempt to offer a trade-off between both physicochemical and empirical modeling approaches.

3.2.1. Varying stress factors and model discretization

Both empirical and semi-empirical models are typically fit to data from cell aging studies. These studies are run with multiple cells that are subjected to varying stress factors. While the stress factors such as temperature or charge–discharge rate vary from cell to cell, stress factors are usually kept constant for a given cell throughout the duration of the study, e.g. one cell stored at 25 °C and others at 35 °C and 45 °C [15,54]. Check-up tests are run after a specific amount of time or cycles for the cells to determine the remaining capacity and other relevant parameters such as the cell impedance. The models are then fit to the resulting data set. Contrary to this, outside-the-lab applications subject the cells to varying external stress factors [25,110]. Some studies age individual cells with varying stress factors to validate the resulting model [17–19]. This model validation at varying stress factors is of importance, since aging mechanisms may show path dependence, i.e. dependence on the order in which a cell has been subjected to different calendar and cyclic stress factors [111,112].

To apply a degradation model with a continuous function, such as $Q_{\text{loss}}^{\text{cal}} = \alpha_T * \alpha_{\text{SOC}} * t^{0.5}$ from Table 2 to varying stress factors, methods for discretization are needed in order to determine the degradation rate for each calculation step. Multiple authors propose to determine the present degradation rate based on the past capacity loss, rather than the past time or energy throughput [16,18,90]. This concept is highlighted in Fig. 8. Assume a cell has been stored at SOC_2 for a specific amount of time t' and accrued a calendar capacity loss of $Q_{\text{loss}}^{\text{cal}\prime}$, see point **A** in Fig. 8. The SOC is then increased to SOC_3, with $\text{SOC}_3 > \text{SOC}_2$. Instead of using the degradation rate at t' for the following calculation time step (point **B**), the higher degradation rate at t_{virtual} is applied (point **C**). The virtual time t_{virtual} refers to the time that had needed to pass for the cell to reach the capacity loss in point **C**. It is calculated by forming the inverse of the capacity loss function, cf. Eq. (8):

$$t_{\text{virtual}} = {Q_{loss}^{cal}}^{-1}(Q_{loss}^{cal\prime}, \text{SOC}_2) \tag{8}$$

The physical rationale behind this concept is that the SEI growth rate is more correlated to the present thickness of the SEI, which manifests itself in capacity loss, than to the amount of time that has passed.

The same principle can be applied to cyclic aging as well, by calculating a virtual number of FECs or charge throughput [19]. Discretization of cyclic aging brings additional complexity though: cycle counting. While calendar aging can be evaluated after every timestep, computing cyclic capacity loss requires a definition of when a cycle is completed. A full charge–discharge cycle from 0% to 100% back to 0% SOC should be computed as one FEC at 100% DOC instead of ten cycles at 10% DOC. Naumann et al. as well as He et al. employ a half cycle counting algorithm in which a cycle is evaluated after every change of charge–discharge direction [19,80]. After such a cycle is detected, DOC and C_{rate} are determined and the cyclic capacity loss is calculated. Another algorithm used for cycle counting is the rainflow-counting algorithm, which is commonly employed in material fatigue analysis [113,114]. It sequences a data series of local maxima and minima into cycle loops and thereby allows to identify individual cycles, their DOC, and C_{rate} in a SOC profile [82,115].

3.2.2. Model requirements and examples

This section provided an overview of common degradation models and in doing so highlighted the significant variety in modeling approaches. To use degradation models for scheduling purposes, we identify four main requirements:

- **Modeling of varying stress factors:** To apply a model to real life use cases, it should include a validated method to represent varying stress factors.
- **Modeling of application relevant stress factors:** The stress factors that are relevant for a given application, should be represented in the model. For the semi-empirical models highlighted in Table 2, all consider the dependence of cyclic aging on DOC, but only some the dependence on C_{rate} and $\overline{SOC}$.
- **Validity for operation range and conditions:** A degradation model that is intended to be used for a given application should be validated for that application's operation range. For example, if an application shows a large amount of cycles at low DOC and high C_{rate}, this should be part of the test conditions through suitable design of experiment.
- **Sufficient computational efficiency:** Sufficient computational efficiency is needed to include degradation models in common scheduling methods.

Individual contributions can be found that aim to provide models specifically for use in battery operation and scheduling [87,114,116,117]. Muenzel et al. proposed a cycle life model that accounts for the cyclic stress factors of C_{rate}, DOC, T, $\overline{SOC}$ and uses the rainflow algorithm for cycle counting [114]. Shi et al. only consider DOC as a stress factor for cyclic aging, but prove convexity of their resulting model which is beneficial for a number of scheduling methods [116].

4. Aging aware operation

In this section, we move from degradation models to aging aware operation strategies. The process of deriving a schedule of charge and discharge signals for a BESS under consideration of technical constraints and economic benefit is referred to with multiple terms in literature: energy management [23], scheduling [39], control [37], dispatch [118] or operation [85]. In the following, we will refer to this general process as scheduling and provide an overview of scheduling methods in Section 4.1. In Section 4.2 we provide a tabular review of contributions that account for battery degradation during scheduling and perform a taxonomy of "aging awareness methods", meaning methods for how to internalize battery degradation into the scheduling method. In Section 4.3 we investigate through time-series simulations which aging stress factors are particularly relevant for selected applications of BESSs.

Fig. 9 summarizes selected key applications of BESSs, which are referenced again in later subsections. **SCI** is often a primary application for residential storage systems and refers to increasing one's own consumption of self generated renewable energy, mostly photovoltaic (PV), by charging energy into the BESS instead of feeding it into the grid in times of excess PV generation. Since electricity costs often exceed remuneration for feeding PV generated electricity into the grid, a net benefit is gained by using the energy from the BESS, once the household load exceeds PV generation again [119]. **Peak shaving (PS)** means smoothing a load profile by discharging the BESS into the load peak and thereby reducing demand charges for an industrial electricity consumer [33]. **Energy arbitrage (EA)** is the process of buying electricity at low prices and selling it at high prices on the respective energy markets. **Balancing power (BP)** describes a grid service in which a BESS provides its power capability to charge during grid over-frequency and discharge during under-frequency, in order to stabilize the electricity grid [36]. Remuneration is handled on the respective power markets, such as the central European auction for frequency containment reserve (FCR) or firm frequency response (FFR) in the United Kingdom. **Microgrid** refers to applications in which a BESS is used to form a microgrid in partial or full independence from larger national electricity grids [82]. In **multi-use** applications, a BESS is used for not one, but multiple of the aforementioned applications by either running them sequentially one after another or in parallel [2]. Lastly, **vehicle-to-grid (V2G)** is the concept of using electric vehicles to fulfill any of the aforementioned applications, including multi-use, through controlled or bi-directional charging [120]. Further applications of BESSs include the provision of backup power, time arbitrage for time-of-use tariffs, as well as transmission & distribution grid upgrade deferral [1].

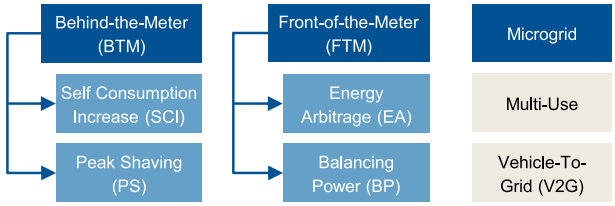

Fig. 9. Overview of key BESS applications. Multi-use and V2G are overarching concepts that can include BTM, FTM or microgrid applications.

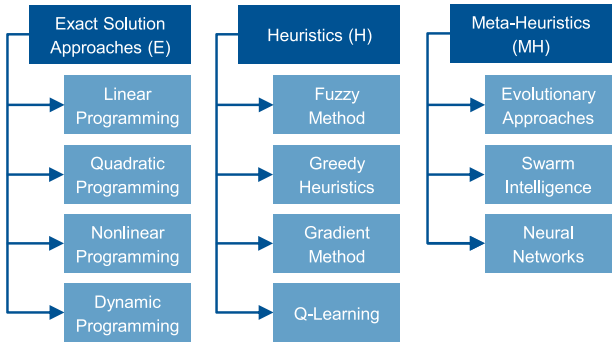

Fig. 10. Non-exhaustive overview of optimization based scheduling methods and their classification.

4.1. Scheduling methods

To operate an energy storage system as optimally as possible, several aspects must be taken into account. In addition to the design of the storage system and the definition of the applications to be served, system constraints, operating expenses, degradation and efficiency have to be considered [85]. In terms of scheduling methods, a distinction is made between rule-based and optimized operation strategies. Rule-based methods offer the advantage of relatively low computational complexity, e.g. discharging a BESS during load peaks in PS operation up to a peak shaving limit and charging it again after the load peak. Optimization based scheduling methods, on the other hand, aim to determine the optimum of an objective function, which is also referred to as the fitting or reward function. Based on literature, optimized operation strategies can be divided into three categories of algorithms: **exact solution approaches (E)**, **heuristics (H)**, and **meta-heuristics (MH)** (cf. Fig. 10) [23].

4.1.1. Exact solution approaches

The most common group of algorithms for optimization based BESS scheduling is exact solution approaches [23]. As the name suggests, this group of algorithms generally has the property of finding the optimal solution to a given optimization problem. It includes linear, nonlinear, and quadratic problems. Often, these standard categories also include extensions with mixed integer problems. A mixed integer linear programming (MILP) problem is an optimization problem that includes

a linear objective function and linear constraints with integer as well as continuous decision variables. Analogously, mixed integer quadratic programming refers to a problem with a quadratic objective function and integer as well as continuous decision variables. In addition to the standard solution approaches for these problem types, such as the simplex algorithm and branch and bound methods, there are decomposition based methods, such as dynamic programming (DP), which are especially used for sequential decisions [121]. While they allow to find the global optimum to a problem, exact solution approaches have the disadvantage that solving them can be computationally expensive. Especially nonlinear programming (NLP) approaches with multiple decision variables can be elaborate and time consuming to solve, which can explain why the faster linear approaches are more frequent in the field of time-series optimization and energy storage [23]. In order to include nonlinear relationships, such as efficiency curves or aging models in a linear scheduling method, linearization approaches are commonly used [33,85]. It should be underlined though, that linearization of models will introduce errors and thereby decrease accuracy [122].

4.1.2. Heuristics

The second group of optimization based scheduling methods are heuristics, which include algorithms, such as the fuzzy method, greedy heuristic, gradient method, and reinforcement learning [23]. Compared to exact solution approaches, heuristics are fast, but have the disadvantage that they can get stuck in local optima [123]. Because of their advantage of relatively fast computing times, heuristics are able to bundle complex nonlinear relationships in an optimization problem. In the work by Cao et al. the reinforcement learning method was used to control an energy storage system during arbitrage trading, while considering battery degradation, charge–discharge efficiency, and market price prediction [38].

4.1.3. Meta-heuristics

In contrast to heuristic approaches, meta-heuristics can be described as heuristics that are allowed a step-wise worsening of the optimization objective, with the intention to avoid local optima [23]. Well-known representatives of meta-heuristics are methods such as evolutionary approaches, swarm intelligence, and neural networks. In Engels et al. a genetic algorithm is presented to determine the optimal scheduling of a large-scale storage system in the German frequency containment reserve market [36]. Comparing this algorithm with other gradient-free global optimization algorithms, the authors found that the chosen differential evolution method converges relatively fast towards the optimization bounds, while allowing the co-optimization of the degradation costs [36]. Other promising candidates for meta-heuristics are swarm intelligence-based search techniques. Hossain et al. and Li et al. used particle swarm optimization (PSO) in the context of microgrid communities and bi-directional electric vehicles, respectively [82,120]. In both approaches, the degradation is actively considered in the fitness functions of the optimization method and the degradation model was implemented with a rain-flow algorithm to determine the energy throughput at the mobile and stationary energy storage systems [82,120]. Liu et al. used a electrothermal-aging model for their optimization problem, that captures the nonlinear electrical, thermal, and degradation dynamics of a lithium-ion battery and solve it using the NSGA-II algorithm [35]. Here, it was found that the chosen genetic algorithm is a viable candidate to determine the optimal operation strategy, allowing the modeling of nonlinear processes as well as hard constraints in the optimization algorithm [35].

4.1.4. Aging aware scheduling example

In general, it can be said that the more detailed the degradation model is, the more complex it is to find a suitable scheduling method. As the literature review shows that degradation aware scheduling methods are largely implemented with MILP algorithms (cf. Tables 4–7 in the following subsection), an example is provided in the following.

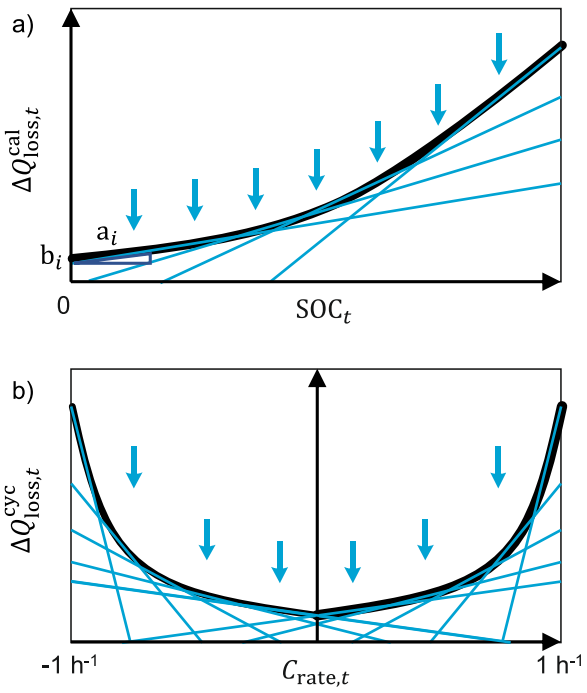

Fig. 11. Exemplary dependency between SOC, C_{rate} and the respective degradation cost. The blue lines depict the linearization and the blue arrows illustrate the minimization of aging costs. (For interpretation of the references to color in this figure legend, the reader is referred to the web version of this article.)

Eq. (9) shows an exemplary objective function, which maximizes the profit $\mathbb{P}$ of the system while accounting for the cost of degradation $\mathbb{C}^{aging}$. In order to limit the solution space of the optimization problem, constraints must be defined (cf. Eqs. (10)–(12)). As shown in Eq. (10), the cost of battery cell degradation at time step t is composed of the capacity loss change from calendar ΔQ^{cal}_{loss} and cyclic ΔQ^{cyc}_{loss} aging, multiplied by the specific aging cost per unit of capacity loss c_{aging}. Further constraints, which are not detailed here, then model how the profit $\mathbb{P}_t$ relates to the charge–discharge rate $C_{rate,t}$ in the given application and how SOC_t changes based on $C_{rate,t}$.

$$\max \sum_{t \in T} \left(\mathbb{P}_t(C_{rate,t}) - \mathbb{C}^{aging}_t \right) \tag{9}$$

$$\mathbb{C}^{aging}_t = (\Delta Q^{cal}_{loss,t}(SOC_t) + \Delta Q^{cyc}_{loss,t}(C_{rate,t})) * c_{aging} \quad \forall t \in T \tag{10}$$

$$Q^{cal}_{loss,t} \geq a_i \cdot SOC_t + b_i \quad \forall i \in I, \forall t \in T \tag{11}$$

$$Q^{cyc}_{loss,t} \geq c_j \cdot C_{rate,t} + d_j \quad \forall j \in J, \forall t \in T \tag{12}$$

This generic example includes a simplified degradation model with two calendar aging stress factors, t and SOC, and two cyclic aging stress factors, FEC and C_{rate}. As discussed in Section 2.2, the usable capacity of lithium-ion cells usually degrades faster at high SOCs. For approximation purposes, the SOC-related stress behavior can be mathematically described with a respective function (cf. thick black line in Fig. 11a). To include this nonlinear degradation behavior in a MILP, linearization techniques are required. By applying the method of linearization, the nonlinear behavior can be step-wise linearized. As shown in Fig. 11a, the nonlinear function is partitioned into $i \in I$ linear functions with slope a_i and y-axis intercept b_i (cf. Eq. (11)). With battery degradation cost $\mathbb{C}^{aging}_t$ included as a penalty factor in the objective function (cf. Eq. (9)), the solver will account for and

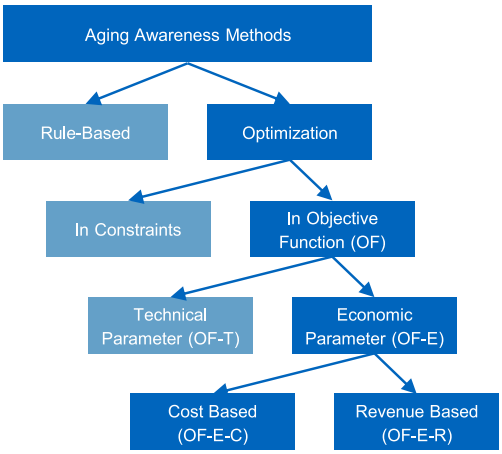

Fig. 12. Categorization of aging awareness methods.

reduce this stress factor (cf. blue arrows in Fig. 11a) and thus avoid higher SOC levels. Analogously, one can also apply linearizations for the C_{rate} in order to approximate this nonlinear stress characteristic that leads to higher degradation costs for increased C_{rate} values (cf. Fig. 11b). In Eq. (12), c_j and d_j respectively represent the slope and y-axis intercept for the set of linear functions $j \in J$ for the $C_{rate,t}$ stress factor. Note that a higher $C_{rate,t}$ will also lead to a larger number of FECs for that timestep. This means that both cyclic aging stress factors, FEC and C_{rate}, can be represented by one set of linear functions, as illustrated by the steep increase of $Q^{cyc}_{loss,t}$ in both charge and discharge direction in Fig. 11b.

4.2. Aging awareness methods

Tables 4 to 7 summarize existing publications in the field of aging aware BESS operation. Next to the scheduling method, application, aging model, and stress factors, the method used to account for battery degradation in the operation strategy is highlighted. A variety of such methods, that we refer to as aging awareness methods, can be found in literature and categorized as in Fig. 12. In summary, these aging awareness methods might negatively effect short-term profitability, but are expected increase long-term profitability by extending the BESS lifetime.

Rule-based approach: We make the first differentiation with regards to the scheduling methods themselves. Rule-based scheduling methods employ rule-based methods as well to limit degradation, while optimization based scheduling strategies provide a wider range of methods. As for rule-based aging awareness methods, Angenendt et al. proposed a forecast based method [119]. Here, a residential storage system is charged up only to the energy level during the day that is forecasted to be needed at night. Thereby the average SOC and calendar aging are reduced. A decrease in levelized cost of electricity of up to 12% is reported as a result [119].

Optimization approach: The majority of scheduling methods are optimization based. The target is to minimize or maximize an objective function through either exact solution approaches, heuristics or meta-heuristics. For those scheduling methods, aging awareness may be induced through constraints, through the objective function or through both.

In Constraints: By setting fixed constraints for the aging stress factors in an optimization problem, the extent of degradation can be reduced. Li et al. limited the C_{rate} through fixed constraints for the charge and discharge power and induce upper and lower limits for the SOC range [120]. Wankmuller et al. limited the SOC range to 60% of the original battery capacity and investigate the techno-economic impact of different limits for the C_{rate} as part of their analysis [124]. Shi et al. limited the usable SOC range to 70% of the original battery capacity [116]. It should be noted that introducing limits for the SOC in an optimization problem will affect the maximum DOC as well. The effects of limiting DOC in different SOC ranges were studied by Perez et al. in a multi-use balancing power and energy arbitrage application [125]. It was found that for the optimal SOC range, the annual average gross revenue is reduced by 18%, but the BESS lifespan is expected to double [125].

A different kind of aging aware constraints was used by Cardoso et al. [126]. Here, an energy throughput limit for the BESS was introduced, which is calculated based on a semi-empirical aging model with the target lifetime and tolerable capacity loss before EOL as inputs [126]. Notably, Cardoso et al. considered both scheduling and system sizing in their optimization framework [126].

Objective Function (OF): Instead of solely relying on constraints, the majority of investigated studies account for degradation directly in the objective function with a penalty factor, as either a Technical Parameter (OF-T) or Economic Parameter (OF-E).

Technical Parameter (OF-T): Multi-objective approaches allow to include technical parameters in the objective function alongside economic parameters for the profit gained in an application. Li et al. directly optimized the sum of all cycles and half-cycles in the objective function for the investigated V2G application [120]. Maheshwari et al. proposed an optimization framework that includes a detailed empirical degradation model for energy arbitrage applications [85]. They used a multi-objective approach, in which revenue and degradation are linked through a weighting factor that should be chosen by the operator. With a lower weighting factor, battery degradation decreases, but so does the short-term revenue that is gained through energy arbitrage [85]. Analogously, with the multi-objective approach by Li et al. the annual cashflow for a residential BESS in their case study decreases from 318 € to 312 €, but the expected lifetime increases from 12 to 15 years [127].

Economic Parameter (OF-E): A significantly larger subset of publications are using a form of economic parameter to link battery degradation with the profit that is generated from the primary applications of the BESS. This is done by either directly assigning a monetary value to degradation in the form of aging cost or by formulating future profit as a function of the expected battery lifetime.

Cost Based (OF-E-C): Two definitions are especially common for aging cost $\mathbb{C}^{aging}$, which are given in Eqs. (13) and (14).

$$\mathbb{C}^{aging}_{SOH} = \frac{c_{battery} * E_n}{1 - SOH_{EOL}} * \Delta SOH \tag{13}$$

In Eq. (13), the aging cost $\mathbb{C}^{aging}_{SOH}$ is calculated based on the specific battery cost $c_{battery}$, the nominal battery capacity at the beginning of life E_n in Wh, the SOH threshold for the end of life SOH_{EOL} and the decrease in SOH (ΔSOH), as proposed by multiple authors [34,36,118,122,128]. In this context, $c_{battery}$ is often chosen as the installation or replacement cost for the full BESS or for just the battery cells. For SOH_{EOL}, 70% [34] or 80% [36,118,122,128] are typical assumptions. As in the example from Section 4.1.4, $\mathbb{C}^{aging}_{SOH}$ is then added to the objective function and ΔSOH is linked to the degradation model through constraints.

$$\mathbb{C}^{aging}_{FEC} = \frac{c_{battery} * E_n}{FEC_{EOL}} * \Delta FEC \tag{14}$$

In Eq. (14), the expected number of full equivalent cycles until EOL FEC_{EOL} and the increase in full equivalent cycles ΔFEC are used to calculate the aging cost $\mathbb{C}^{aging}_{FEC}$, as also proposed by multiple authors [2,83,84,116,129]. Here, FEC_{EOL} can be constant or linked to the degradation model, the latter often making the model nonlinear.

With such aging cost in the objective function, Englberger et al. reported a system lifetime increase from 2.4 to 8.6 years and a profitability index increase over its lifetime from 0.06 to 1.24 [2], for the investigated multi-use application. Weitzel et al. reported a lifetime

Table 4
Scheduling methods that are using technical parameters (OF-T) or reward based economic parameters (OF-E-R) within the objective function.

Reference	Aging awareness method[a]	Aging model types[b]	FEC	DOC	C_{rate}	$\overline{SOC}$	T_{cyc}	t	SOC	T_{cal}	Scheduling method	Applications
Li [127]	**OF-T:** Calendar capacity loss in OF, linked to economic benefit through weighting factors	Semi-Empirical [86]						×	×	×	E: DP	SCI
Maheshwari [85]	**OF-T:** Cyclic capacity loss in OF, linked to economic benefit through weighting factors	Empirical [94]	×	×	×	×					E: MILP	EA
He [80]	**OF-E-R:** Profit maximization based on expected lifetime in days times projected profit per day	Empirical	×	×				×			E: NLP	EA & BP
Abdulla [130]	**OF-E-R:** Penalty factor based on the cumulative degradation and expected lifetime cost savings generated through the BESS	Empirical [114]	×	×	×	×		×			E: DP	SCI
Liu [35]	**OF-E-R:** Penalty factor based on the expected cycles until EOL and battery resale value	Semi-Empirical [117]	×	×	×	×	×				MH: NSGA-II	V2G

[a]Aging Awareness Method Abbreviations: Technical Parameter in Objective Function (OF-T), Cost Based Economic Parameter in Objective Function (OF-E-C), Revenue Based Economic Parameter in Objective Function (OF-E-R).

[b]For each aging model, the cyclic (FEC, DOC, C_{rate}, $\overline{SOC}$, T_{cyc}) and calendar (t, SOC, T_{cal}) stress factors are marked by "×" if they are internalized into the listed scheduling method.

increase from 6.9 to 12 years in the investigated microgrid application by adding aging cost to the objective function [122].

As Eqs. (13) and (14) show, the assumption for the EOL criterion significantly influences the aging cost and thereby the optimized operation strategy. Hou et al. investigated in more detail the affect of the EOL criterion and propose an alternative efficiency-based criterion in their optimization model [33].

Instead of deriving the aging cost directly from battery cost as in Eqs. (13) and (14), Wankmuller et al. investigated the impact of varying aging cost values through parameter variation in a MILP [124]. They concluded that a penalty factor of 100 $ per kWh of capacity loss leads to the highest total profit in the investigated energy arbitrage application over the BESS lifetime, when assuming EOL at either 80% remaining capacity or after 10 years of operation. It is worth pointing out that 100 $ per kWh of capacity loss is significantly lower than the commonly assumed costs for battery replacement or installation $c_{battery}$ in other published aging aware operation strategies, in the range of 250 to 500 € per kWh [36,118].

Revenue Based (OF-C-R): While cost based methods include some form of aging cost as a penalty factor, revenue based methods create a link between revenue and degradation behavior in the objective function. Liu et al. added the degradation dependent future resale value of the battery to the objective function [35]. Abdulla et al. used cumulative past savings that were generated by the BESS to determine a monetary value for capacity loss [130]. They also investigated the influence of the forecasting errors on their stochastic DP. Intuitively, the revenue generated in the application is higher with the simplified assumption of perfect foresight than with their multiple linear regression forecast for power demand and power generation. The lifetime increases from their reference case of basic set point control (4 years predicted lifetime) to stochastic DP (11 years predicted lifetime) was reported to be the same though for both perfect foresight and the multiple linear regression forecast [130]. Lastly, He et al. multiplied the projected daily revenue with the expected lifetime in days, based on an empirical degradation model, as part of a nonlinear programming approach [80]. Here, with consideration of battery cycle life, daily revenue decreased by 19.2%, but the expected lifetime increases from 6.3 to 10 years [80].

4.3. Application specific relevance of stress factors

In this section, the relevance of calendar and cyclic stress factors for different applications is investigated. For that purpose, we use the inhouse developed open-source Simulation Tool for Stationary Energy Storage Systems (**SimSES**) [143]. **SimSES** can be used to conduct time-series simulations for energy storage systems in various applications. A variety of battery storage technologies and peripheral components are available. The simulation tool allows a detailed techno-economic analysis following the simulation. This includes an analysis of calendar and cyclic capacity loss, which is in focus here.

For this review, BESSs with NMC and LFP lithium-ion batteries are simulated in the previously introduced applications FCR, SCI and PS. The cell and aging model of the NMC type battery are based on the work of Schmalstieg et al. [15] and those of the LFP battery are based on Naumann et al. [18,19] (cf. Table 2 for the degradation models). For each application, input profiles are used: a grid frequency profile for FCR, a household load profile and a PV generation profile for SCI and an industrial load profile for PS. The BESSs are dimensioned analogously to Kucevic et al. [25]. For the power electronics, the model of an AC/DC converter measured by Notton et al. is used [140]. In addition, 25 ° C is chosen as fixed cell temperature to ensure comparability between the three applications, irrespective of the thermal design of each system. The simulation parameters are summarized in Table 8.

First, we investigate the distribution of calendar and cyclic stress factors for the three applications (FCR, SCI, PS) and their effect on cell degradation for the two investigated degradation models (LFP Naumann and NMC Schmalstieg): Fig. 13 shows the resulting calendar and cyclic stress factors. FCR is characterized by an average SOC around 50% with a large amount of cycles at low DOC and C_{rate}, following the BESS response to the fluctuating grid frequency. In SCI, the BESS spends a large amount of time at 100% SOC after being fully charged by the PV system and 0% SOC after discharging all its energy to cover the household load, once the household load exceeds PV production again. Compared to the other two applications, SCI requires more cycles at a higher DOC and C_{rate}. Lastly, in PS the BESS is fully charged in anticipation of a possible load peak for the majority of time, while being subjected to few cycles.

Table 5
Scheduling methods that are using cost based economic parameters within objective function (OF-E-C) Part I.

Reference	Aging awareness method	Aging model types	FEC	DOC	C_{rate}	$\overline{SOC}$	T_{cyc}	t	SOC	T_{cal}	Scheduling Method	Applications
Kazemi [81]	**OF-E-C:** Aging cost per day based on battery cost divided by the expected lifetime in days	Empirical	×	×							E: Benders Decomposition	EA & BP
Engels [36]	**OF-E-C:** Aging cost based on capacity loss times battery cost, assuming EOL at 80%	Semi-Empirical [15]	×	×		×		×	×	×	MH: Differential Evolution Algorithm	BP
Hesse [118]	**OF-E-C:** Aging cost based on capacity loss times battery cost, assuming EOL at 80%	Semi-Empirical [54]	×		×			×	×		E: MILP	EA & BP
Weitzel [122]	**OF-E-C:** Aging cost based on capacity loss times BESS investment cost, assuming EOL at 80%	Semi-Empirical [16,17]	×	×				×	×		E: MILP	Microgrid
Kruger [128]	**OF-E-C:** Aging cost based on future discounted replacement cost, assuming EOL at 80%	Semi-Empirical [90]	×		×			×	×		E: MILP	SCI
Cao [38]	**OF-E-C:** Aging cost based on capacity loss times battery cost	Semi-Empirical [87]	×	×		×	×	×	×	×	H: Reinforcement Learning	EA
Cai [34]	**OF-E-C:** Aging cost based on capacity loss times battery cost, assuming EOL at 70%	Physicochemical[a] [131]	×	×	×			×	×		E: NLP (Convex)	SCI
Reniers [37]	**OF-E-C:** Aging cost based on capacity loss times different penalty factors in € per kWh capacity loss	x: Empirical y: Semi-Empirical [15] z: Physicochemical[b]	xyz	yz	yz	z	z	yz	yz	yz	E: Linear & Nonlinear Programming	EA

[a]The physicochemical model in [34] considers SEI growth and active material loss. It is linearized and not directly embedded in the optimization problem.
[b]While the physicochemical model in [37] is dependent on all mentioned stress factors, the only aging mechanisms modeled is SEI growth.

Table 6
Scheduling methods that are using cost based economic parameters within objective function (OF-E-C) Part II.

Reference	Aging awareness method	Aging model types	FEC	DOC	C_{rate}	$\overline{SOC}$	T_{cyc}	t	SOC	T_{cal}	Scheduling Method	Applications
Hossain [82]	**OF-E-C:** Aging cost based on relative amount of used cycles times investment cost	Empirical	×	×							MH: PSO	Microgrid
Shi [83]	**OF-E-C:** Aging cost based on relative amount of used cycles times replacement cost	Empirical	×	×							E: NLP (Convex)	BP
Padmanabhan [84]	**OF-E-C:** Aging cost based on relative amount of used cycles times battery cost	Empirical [132]	×	×	×						E: MILP	EA & BP
Kim [129]	**OF-E-C:** Aging cost based on relative amount of used cycles times installation cost	Empirical [133]	×	×		×					E: DP	Generic
Englberger [2]	**OF-E-C:** Aging cost based on relative amount of used cycles times investment cost	Semi-Empirical [15]	×	(×)[a]		(×)		(×)	(×)	(×)	E: MILP	Multi-Use
Hou [33]	**OF-E-C:** Aging cost based on relative amount of used cycles times investment cost, efficiency based criterion for EOL	Semi-Empirical [15]	×	×							E: MILP	PS
Zia [134]	**OF-E-C:** Aging cost based on investment cost, O&M cost and battery residual value, divided by scaling factors to account for degradation	Empirical	×	×			×				E: NLP	Microgrid

[a]For stress factor entries marked with "(×)" instead of "×", the stress factors are not directly integrated into the scheduling method, but used for validation of the scheduling results in a separate model.

Fig. 14 shows the resulting calendar and cyclic capacity loss in the respective applications for the LFP Naumann and NMC Schmalstieg models after 5 years. It can be seen that the LFP model has a higher cycle stability than the NMC model, while the NMC model shows less calendar aging than the LFP model. In the FCR application, the calendar capacity loss predominates for the LFP battery due to the small DOCs and C_{rate}. For the NMC battery, the calendar aging also predominates slightly. SCI is the application with the largest cyclic capacity loss for both models. The extremely high cyclic capacity loss for the NMC model can be explained through the stress factor $\beta_{\overline{V_{cell}}} = \gamma_1 * (\overline{V_{cell}} - \gamma_2)^2$ (cf. Table 2): in the SCI application a large amount of FECs are conducted at high or low cell voltage, with the battery being

Table 7
Scheduling methods that employ a rule-based aging awareness method or that are using constraints within the optimization problem.

Reference	Aging awareness method	Aging model types	FEC	DOC	C_{rate}	$\overline{SOC}$	T_{cyc}	t	SOC	T_{cal}	Scheduling Method	Applications
Angenendt [119]	**Rule-based:** Reduction of average SOC through load forecasting	Semi-Empirical [135]	(×)	(×)		(×)		(×)	(×)	(×)	Rule-based	SCI
Perez [125]	**In Constraints:** Varying upper and lower limits for the usable SOC range	Empirical [136]	(×)	×	(×)						E: MILP	EA & BP
Cardoso [126]	**In Constraints:** Limit for the energy throughput based on the target lifetime and the expected operating temperature	Semi-Empirical [137]	×		(×)			×		(×)	E: MILP	Microgrid
Li [120]	**In Constraints:** upper and lower limits for SOC and C_{rate} **OF-T:** Minimization of total FECs	Empirical	×		×	×					MH: PSO	V2G
Wankmuller [124]	**In Constraints:** upper and lower limits for SOC and C_{rate} **OF-E-C:** Aging cost as penalty factor with optimal value as subject the investigation	Empirical [138,139]	×								E: MILP	EA
Shi [116]	**In Constraints:** upper and lower limits for SOC **OF-E-C:** Aging cost as penalty factor based on battery cost and cycles until EOL	Empirical	×	×							E: NLP (Convex)	Multi-Use

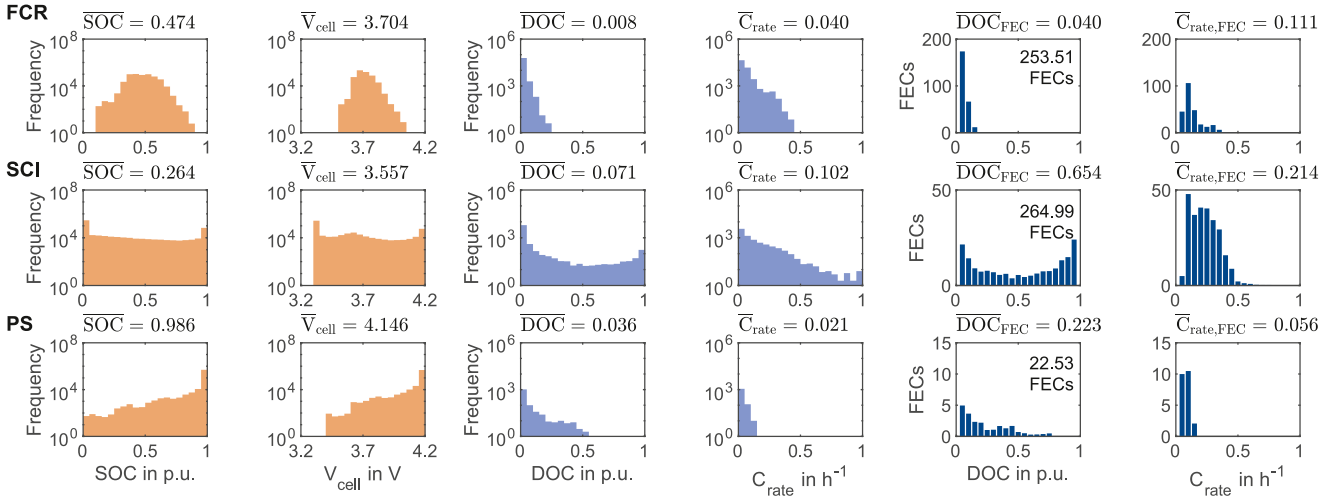

Fig. 13. Distribution and averages of calendar and cyclic stress factors for the three investigated applications (1 year simulation): frequency containment reserve (FCR - top), self consumption increase (SCI - mid), and peak shaving (PS - bottom), based on a one year simulation with the NMC Schmalstieg [15] model at 60 s timesteps. The left two columns (orange) show the frequency of the calendar stress factors, the mid two columns the frequency of the cyclic stress factors (light blue) and the right two columns (dark blue) show the amount of FECs conducted with the cyclic stress factors. Note the logarithmic y-axis for the left four columns of plots. (For interpretation of the references to color in this figure legend, the reader is referred to the web version of this article.)

either empty or full the majority of time, leading to high values for this stress factor with $\gamma_2 = 3.725$ V. Lastly, for the PS application, calendar capacity loss dominates for both models due to the high average SOC / V_{cell} and low amount of FECs.

Often, only a subset of all stress factors are tested in an aging study (cf. Table 2). For example, Schmalstieg et al. cycled all cells at C_{rate} of 1 h^{-1} [15]. While the model by Naumann et al. includes variations in C_{rate}, it does not account for the cyclic stress factor of $\overline{SOC}$ [19]. An even smaller subset of stress factors is considered in most scheduling methods (cf. Tables 4–7). In order to give an estimate of the expected modeling errors due to neglect of individual stress factors in the cell aging study or scheduling method, a series of case studies is conducted hereafter: As a reference case, the NMC Schmalstieg and LFP Naumann models are simulated with all stress factors for FCR, SCI and PS over five years. In the second case, simulations are carried out where for each run one of the stress factors is set to a fixed value that is typically used in an aging study if the dependence of that stress factor is not explicitly modeled. The other stress factors are explicitly calculated as per the aging models. Here, we assume for the LFP Naumann model a DOC of 5%, a C_{rate} of 1 h^{-1} and a SOC of 50%. For the NMC Schmalstieg model, we assume a DOC of 5% as well as a V_{cell} and $\overline{V_{cell}}$ of 3.7136 V, which equals a SOC of 50% as per its open circuit voltage curve. This scenario is referred to as **"typical in aging study"** in the following. In the third case, in each simulation an average value for the respective stress factor is assumed, in order to elaborate if doing so is a valid

Table 8
Application-specific data and profiles for the case study.

Application	FCR	SCI	PS
Storage capacity	1.6 MWh	5 kWh	100 kWh
Rated power	1.6 MW	5 kW	40 kW
AC/DC Conv.	Notton [140]	Notton [140]	Notton [140]
Profiles (1 year)	Frequency profile [141]	PV profile [25], household load profile (profile 28 in [142])	Industry load profile (cluster 2 in [25])
Cell/Degradation Models	3 Ah LFP/Naumann et al. [18,19] 2.15 Ah NMC/Schmalstieg et al. [15]		

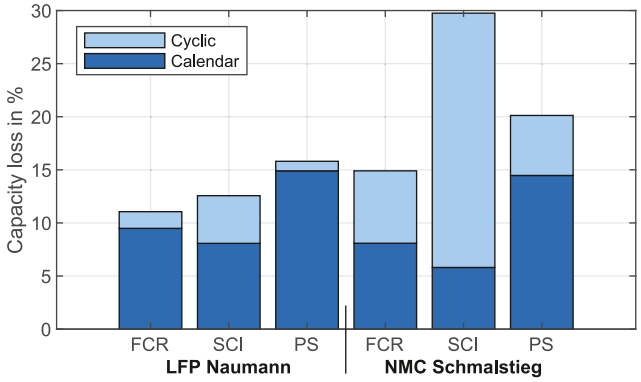

Fig. 14. Capacity loss over five years of the LFP Naumann model (left) and the NMC Schmalstieg model (right) in the BESS applications frequency containment reserve (FCR), self consumption increase (SCI) and peak shaving (PS), split into calendar and cyclic capacity loss. This case is the "standard aging model" in the following figures.

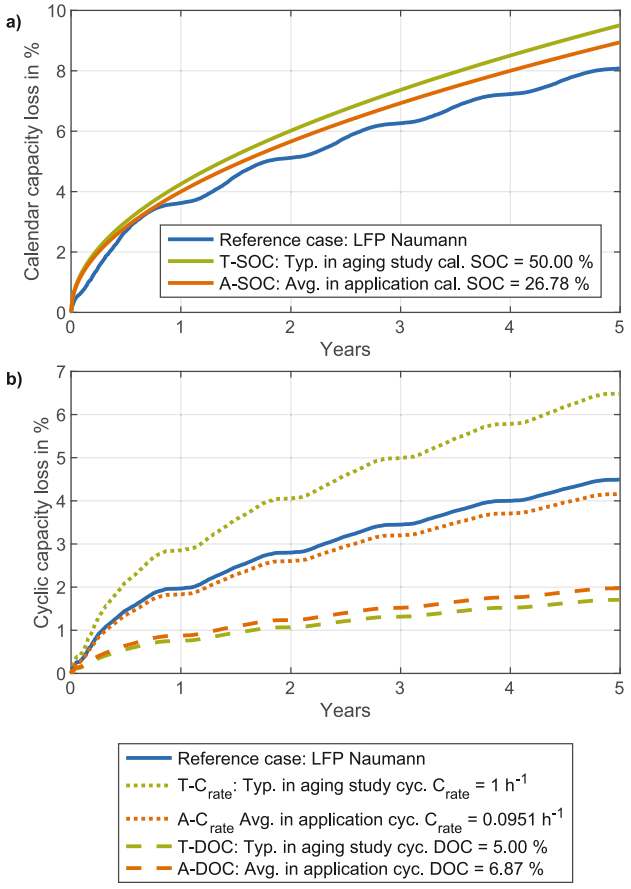

Fig. 15. Calendar capacity loss (a) and cyclic capacity loss (b) for a BESS with the LFP Naumann model in the SCI application over 5 years. The green curves show the results when using typical values from aging studies for the stress factors (SOC = 50%, C_{rate} = 1 h^{-1} and DOC = 5%). The orange curves show the results when using the application-specific averages (SOC = 26.78%, C_{rate} = 0.0951 h^{-1} and DOC = 6.87%). (For interpretation of the references to color in this figure legend, the reader is referred to the web version of this article.)

option over internalizing each stress factor into a scheduling method. This case is referred to as **"average in application"** in the following. The average values are determined based on one year simulations, analogously to Fig. 13, e.g. 7.1% for the DOC in the SCI application with the NMC Schmalstieg model. The results of the capacity loss for the BESS with the LFP Naumann model in the use cases for the SCI application are shown in Fig. 15. An example: in Fig. 15b, calculating the cyclic capacity loss using a constant C_{rate} of 1 h^{-1} (scenario T-C_{rate}) leads to an overestimation of the cyclic capacity loss, while the usage of the average C_{rate} in this application replicates the real cyclic capacity loss well (scenario A-C_{rate}).

In the following, we analyze the deviations of the cases from the standard aging model calculation for the LFP Naumann and NMC Schmalstieg models in the three applications (cf. Fig. 16).

In the FCR application with many small cycles around an SOC of about 50%, the assumption of typical values from aging studies or application specific averages for the SOC or V_{cell} only lead to minor deviations compared to the use of the respective exact values from the reference case. The assumption of fixed values for the C_{rate} and DOC leads to slight deviations, which, however, are in the range of less than one percentage point.

The SCI application shows the greatest deviations overall. The values of the stress factors are widely scattered in this application: The BESS sees time-of-day and seasonal variations in SOC and very small, as well as very large, DOCs. In addition, SOCs and DOCs are also very dependent on the dimensioning of the PV system, the BESS, and the load curve. The largest deviations in the results are found when the average or typical value for the DOC or the typical value for the C_{rate} are used instead of the exact values. This is mainly due to the large variation in DOC in this application.

A BESS in PS application is often in the high SOC range and runs few cycles. As a result, calendar aging is particularly relevant in this application (see Fig. 14). If a fixed SOC of 50% or the corresponding V_{cell} is used here, this leads to large deviations in the capacity loss results. In contrast, using the PS average SOC of around 98% leads to very small deviations, as the SOC of the BESS is often in this range. Average or typical values can also be used for the C_{rate} and DOC, but this leads to small deviations, especially for the NMC Schmalstieg model.

Overall, the evaluation and variation of the stress factors in the applications shows that (a) in FCR, the use of average values for the stress factors leads to only small deviations, attention should be paid though to the low DOC and C_{rate} when selecting a degradation model; (b) in SCI, DOC and C_{rate} are especially relevant; (c) in PS, SOC is the most relevant stress factor, but due to the small variation in operation, an average value may be used without major deviations in the resulting capacity loss.

5. Summary and outlook

This contribution summarizes aging mechanisms, aging stress factors, and degradation modeling approaches for common lithium-ion cell types that are used in BESSs. Furthermore, we review and categorize methods that aim to increase BESS lifetime by accounting for battery degradation effects in the operation strategy. SEI growth on the anode alongside multiple cathode aging mechanisms are the predominant aging mechanisms during the main operation phase. Towards the EOL, cells often show rapid capacity loss, which can be caused

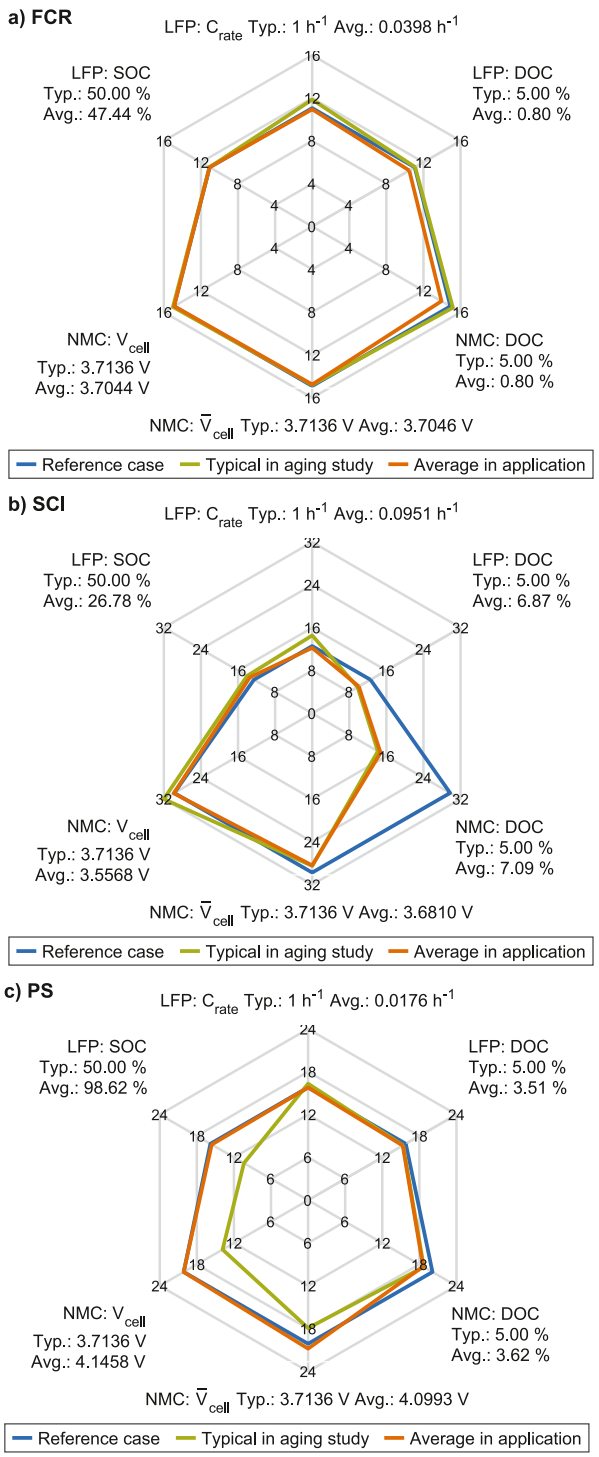

Fig. 16. Spider diagrams of the relative capacity loss for varying the different stress factor scenarios in the applications frequency containment reserve (a), self consumption increase (b) and peak shaving (c). The relative capacity loss is shown after 5 years of simulation time. The top three categories represent the LFP stress factors, the bottom three categories represent the NMC ones. The diagrams show the relative capacity loss using the reference aging model (blue), using typical values from aging studies (green) and using the average values for each application (orange). (For interpretation of the references to color in this figure legend, the reader is referred to the web version of this article.)

by lithium plating or electrolyte depletion. Since the extend of aging depends on external calendar and cyclic stress factors, the degradation behavior can be directly influenced through the operation strategy.

To quantify the resulting capacity loss, empirical, semi-empirical, and physicochemical modeling approaches exist. Present publications in the field of BESS scheduling primarily rely on empirical and semi-empirical modeling approaches, that usually include only a subset of the calendar and cyclic stress factors.

To determine an optimal operation strategy, different scheduling method find use: exact solution approaches, heuristics, and meta-heuristics. The exact solution approach of mixed integer linear programming is particularly frequently used in existing publications. The approaches that are used to account for battery degradation in the scheduling method can be categorized into different aging awareness methods. Most publications rely on a cost based penalty factor for battery degradation, i.e. “aging cost”, that is linked to the economic profit from the BESS application as part of the objective function. The case study in Section 4.3 highlights the difference in aging stress factors for key applications of BESSs and shows the importance of making sure that the key stress factors of an application are represented in the degradation model and considered in the scheduling method.

A number of challenges in the field aging aware operation of BESSs remain open and provide opportunity for future research:

- The degradation models that are used for BESS operation usually do not consider the rapid capacity decrease and change in dominant aging mechanisms towards the EOL. Adapting the charge and discharge cut-off voltage or limiting the C_{rate} further towards the EOL may enable further extension of BESS lifetime.
- Machine learning and filtering methods provide an opportunity to improve aging aware operation strategies over the BESS lifetime. This may be done by adapting the degradation models that are used for scheduling based on field data.
- Capacity loss is usually modeled as part of the scheduling method as the primary effect of battery degradation. Accounting for the resistance increase as well may lead to performance improvements.
- While uncertainty in forecasts for price, load, or PV production are considered in some contributions and addressed through methods such as stochastic programming, the uncertainty in degradation modeling is not considered. Accounting for degradation modeling uncertainty may lead to different optimal strategies for risk-seeking and risk-averse BESS operators.
- Aging costs are often chosen based on the battery installation or replacement cost, to link the short-term scheduling problem to long-term degradation effects. Depending on the system operator’s objective (e.g. maximum profit until EOL at 80% remaining capacity, maximum profit in the next five years, or maximum profit with system replacements for the indefinite future), a different definition of aging cost may lead to the actual optimal long-term result.

Finally, field data from the increasingly growing and aging fleet of globally installed BESSs is likely to lead to further insights into aging aware operation.

CRediT authorship contribution statement

Nils Collath: Conceptualization, Methodology, Writing – original draft, Writing – review & editing, Software, Project administration, Visualization, Investigation. **Benedikt Tepe:** Writing – original draft, Writing – review & editing, Software, Visualization, Investigation. **Stefan Englberger:** Writing – original draft, Writing – review & editing. **Andreas Jossen:** Writing – review & editing, Funding acquisition. **Holger Hesse:** Writing – original draft, Writing – review & editing, Supervision.

Declaration of competing interest

The authors declare that they have no known competing financial interests or personal relationships that could have appeared to influence the work reported in this paper.

Data availability

The adapted version of the open-source software **SimSES** that was used in Section 4.3 and the simulation are available online, hosted by the Technical University of Munich [144]: https://doi.org/10.14459/2022mp1652796

Funding and acknowledgment

This research is funded by the Bavarian Research Foundation via the research project SmartB4P, Germany (reference number AZ-1376-19) as well as by the German Federal Ministry of Education and Research (BMBF) via the research project greenBattNutzung (grant number 03XP0302D). The project greenBattNutzung is overseen by Project Management Juelich (PtJ).

References

[1] M. Killer, M. Farrokhseresht, N.G. Paterakis, Implementation of large-scale Li-ion battery energy storage systems within the EMEA region, Appl. Energy 260 (2020) 114166, http://dx.doi.org/10.1016/j.apenergy.2019.114166.

[2] S. Englberger, A. Jossen, H. Hesse, Unlocking the potential of battery storage with the dynamic stacking of multiple applications, Cell Rep. Phys. Sci. 1 (11) (2020) 100238, http://dx.doi.org/10.1016/j.xcrp.2020.100238.

[3] International Energy Agency, Energy storage: tracking report - november 2021, 2021, URL https://www.iea.org/reports/energy-storage.

[4] International Renewable Energy Agency, Electricity storage and renewables: Costs and markets to 2030, 2017, URL https://www.irena.org/publications/2017/Oct/Electricity-storage-and-renewables-costs-and-markets.

[5] J. Figgener, P. Stenzel, K.-P. Kairies, J. Linßen, D. Haberschusz, O. Wessels, G. Angenendt, M. Robinius, D. Stolten, D.U. Sauer, The development of stationary battery storage systems in Germany – A market review, J. Energy Storage 29 (2020) 101153, http://dx.doi.org/10.1016/j.est.2019.101153.

[6] U.S. Energy Information Administration, Battery storage in the United States: An update on market trends, 2020, URL https://www.eia.gov/analysis/studies/electricity/batterystorage/.

[7] K. Mongrid, Viswanathan Vilayanur, J. Alam, C. Vartanian, V. Sprenkle, 2020 Grid energy storage technology cost and performance assessment, 2020, URL https://www.energy.gov/energy-storage-grand-challenge/downloads/2020-grid-energy-storage-technology-cost-and-performance.

[8] K. Uddin, R. Gough, J. Radcliffe, J. Marco, P. Jennings, Techno-economic analysis of the viability of residential photovoltaic systems using lithium-ion batteries for energy storage in the United Kingdom, Appl. Energy 206 (10) (2017) 12–21, http://dx.doi.org/10.1016/j.apenergy.2017.08.170.

[9] M. Astaneh, R. Roshandel, R. Dufo-López, J.L. Bernal-Agustín, A novel framework for optimization of size and control strategy of lithium-ion battery based off-grid renewable energy systems, Energy Convers. Manage. 175 (Part 1) (2018) 99–111, http://dx.doi.org/10.1016/j.enconman.2018.08.107.

[10] J.S. Edge, S. O'Kane, R. Prosser, N.D. Kirkaldy, A.N. Patel, A. Hales, A. Ghosh, W. Ai, J. Chen, J. Yang, S. Li, M.-C. Pang, L. Bravo Diaz, A. Tomaszewska, M.W. Marzook, K.N. Radhakrishnan, H. Wang, Y. Patel, B. Wu, G.J. Offer, Lithium ion battery degradation: what you need to know, Phys. Chem. Chem. Phys.: PCCP 23 (14) (2021) 8200–8221, http://dx.doi.org/10.1039/d1cp00359c.

[11] J.P. Pender, G. Jha, D.H. Youn, J.M. Ziegler, I. Andoni, E.J. Choi, A. Heller, B.S. Dunn, P.S. Weiss, R.M. Penner, C.B. Mullins, Electrode degradation in lithium-ion batteries, ACS Nano 14 (2) (2020) 1243–1295, http://dx.doi.org/10.1021/acsnano.9b04365.

[12] J. Vetter, P. Novák, M.R. Wagner, C. Veit, K.-C. Möller, J.O. Besenhard, M. Winter, M. Wohlfahrt-Mehrens, C. Vogler, A. Hammouche, Ageing mechanisms in lithium-ion batteries, J. Power Sources 147 (2005) 269–281, http://dx.doi.org/10.1016/j.jpowsour.2005.01.006.

[13] P. Arora, R.E. White, Capacity fade mechanisms and side reactions in lithium–Ion batteries, J. Electrochem. Soc. 145 (1998) 3647–3667, http://dx.doi.org/10.1149/1.1838857.

[14] M. Ecker, J.B. Gerschler, J. Vogel, S. Käbitz, F. Hust, P. Dechent, D.U. Sauer, Development of a lifetime prediction model for lithium-ion batteries, ecker.2based on extended accelerated aging test data, J. Power Sources 215 (2012) 248–257, http://dx.doi.org/10.1016/j.jpowsour.2012.05.012.

[15] J. Schmalstieg, S. Käbitz, M. Ecker, D.U. Sauer, A holistic aging model for Li(NiMnCo)O2 based 18650 lithium-ion batteries, J. Power Sources 257 (2014) 325–334, http://dx.doi.org/10.1016/j.jpowsour.2014.02.012.

[16] E. Sarasketa-Zabala, I. Gandiaga, L.M. Rodriguez-Martinez, I. Villarreal, Calendar ageing analysis of a LiFePO4/graphite cell with dynamic model validations: Towards realistic lifetime predictions, J. Power Sources 272 (2014) 45–57, http://dx.doi.org/10.1016/j.jpowsour.2014.08.051.

[17] E. Sarasketa-Zabala, I. Gandiaga, E. Martinez-Laserna, L.M. Rodriguez-Martinez, I. Villarreal, Cycle ageing analysis of a LiFePO4/graphite cell with dynamic model validations: Towards realistic lifetime predictions, J. Power Sources 275 (2015) 573–587, http://dx.doi.org/10.1016/j.jpowsour.2014.10.153.

[18] M. Naumann, M. Schimpe, P. Keil, H.C. Hesse, A. Jossen, Analysis and modeling of calendar aging of a commercial LiFePO4/graphite cell, J. Energy Storage 17 (2018) 153–169, http://dx.doi.org/10.1016/j.est.2018.01.019.

[19] M. Naumann, F.B. Spingler, A. Jossen, Analysis and modeling of cycle aging of a commercial LiFePO4/graphite cell, J. Power Sources 451 (2020) 227666, http://dx.doi.org/10.1016/j.jpowsour.2019.227666.

[20] X. Han, L. Lu, Y. Zheng, X. Feng, Z. Li, J. Li, M. Ouyang, A review on the key issues of the lithium ion battery degradation among the whole life cycle, ETransportation (2019) http://dx.doi.org/10.1016/j.etran.2019.100005.

[21] S. Pelletier, O. Jabali, G. Laporte, M. Veneroni, Battery degradation and behaviour for electric vehicles: Review and numerical analyses of several models, Transp. Res. B 103 (2017) 158–187, http://dx.doi.org/10.1016/j.trb.2017.01.020.

[22] M. Woody, M. Arbabzadeh, G.M. Lewis, G.A. Keoleian, A. Stefanopoulou, Strategies to limit degradation and maximize Li-ion battery service lifetime - critical review and guidance for stakeholders, J. Energy Storage 28 (2020) http://dx.doi.org/10.1016/j.est.2020.101231.

[23] T. Weitzel, C.H. Glock, Energy management for stationary electric energy storage systems: A systematic literature review, European J. Oper. Res. 264 (2) (2018) 582–606, http://dx.doi.org/10.1016/j.ejor.2017.06.052.

[24] H. Hesse, M. Schimpe, D. Kucevic, A. Jossen, Lithium-ion battery storage for the grid—A review of stationary battery storage system design tailored for applications in modern power grids, Energies 10 (12) (2017) 2107, http://dx.doi.org/10.3390/en10122107.

[25] D. Kucevic, B. Tepe, S. Englberger, A. Parlikar, M. Mühlbauer, O. Bohlen, A. Jossen, H. Hesse, Standard battery energy storage system profiles: Analysis of various applications for stationary energy storage systems using a holistic simulation framework, J. Energy Storage 28 (2020) 101077, http://dx.doi.org/10.1016/j.est.2019.101077.

[26] N. Pinsky, L. Gaillac, A. Mendoza, J. Argueta, T. Knipe, Performance of advanced electric vehicle batteries in stationary applications, in: 24th Annual International Telecommunications Energy Conference, IEEE, 2002, pp. 366–372, http://dx.doi.org/10.1109/INTLEC.2002.1048682.

[27] J. Neubauer, A. Pesaran, The ability of battery second use strategies to impact plug-in electric vehicle prices and serve utility energy storage applications, J. Power Sources 196 (23) (2011) 10351–10358, http://dx.doi.org/10.1016/j.jpowsour.2011.06.053.

[28] E. Martinez-Laserna, I. Gandiaga, E. Sarasketa-Zabala, J. Badeda, D.-I. Stroe, M. Swierczynski, A. Goikoetxea, Battery second life: Hype, hope or reality? A critical review of the state of the art, Renew. Sustain. Energy Rev. 93 (April) (2018) 701–718, http://dx.doi.org/10.1016/j.rser.2018.04.035.

[29] L.C. Casals, B. Amante García, C. Canal, Second life batteries lifespan: Rest of useful life and environmental analysis, J. Environ. Manag. 232 (2019) 354–363, http://dx.doi.org/10.1016/j.jenvman.2018.11.046.

[30] Y. Li, K. Liu, A.M. Foley, A. Zülke, M. Berecibar, E. Nanini-Maury, J. van Mierlo, H.E. Hoster, Data-driven health estimation and lifetime prediction of lithium-ion batteries: A review, Renew. Sustain. Energy Rev. 113 (2019) 109254, http://dx.doi.org/10.1016/j.rser.2019.109254.

[31] J. Reniers, G. Mulder, D. Howey, Review and performance comparison of mechanical-chemical degradation models for lithium-ion batteries, J. Electrochem. Soc. 166 (14) (2019) A3189–A3200, http://dx.doi.org/10.1149/2.0281914jes.

[32] A. Ahmadian, M. Sedghi, A. Elkamel, M. Fowler, M. Aliakbar Golkar, Plug-in electric vehicle batteries degradation modeling for smart grid studies: Review, assessment and conceptual framework, Renew. Sustain. Energy Rev. 81 (2018) 2609–2624, http://dx.doi.org/10.1016/j.rser.2017.06.067.

[33] Q. Hou, Y. Yu, E. Du, H. He, N. Zhang, C. Kang, G. Liu, H. Zhu, Embedding scrapping criterion and degradation model in optimal operation of peak-shaving lithium-ion battery energy storage, Appl. Energy 278 (2020) 115601, http://dx.doi.org/10.1016/j.apenergy.2020.115601.

[34] J. Cai, H. Zhang, X. Jin, Aging-aware predictive control of PV-battery assets in buildings, Appl. Energy 236 (2019) 478–488, http://dx.doi.org/10.1016/j.apenergy.2018.12.003.

[35] K. Liu, X. Hu, Z. Yang, Y. Xie, S. Feng, Lithium-ion battery charging management considering economic costs of electrical energy loss and battery degradation, Energy Convers. Manage. 195 (2019) 167–179, http://dx.doi.org/10.1016/j.enconman.2019.04.065.

[36] J. Engels, B. Claessens, G. Deconinck, Techno-economic analysis and optimal control of battery storage for frequency control services, applied to the German market, Appl. Energy 242 (2019) 1036–1049, http://dx.doi.org/10.1016/j.apenergy.2019.03.128.

[37] J.M. Reniers, G. Mulder, S. Ober-Blöbaum, D.A. Howey, Improving optimal control of grid-connected lithium-ion batteries through more accurate battery and degradation modelling, J. Power Sources 379 (2018) 91–102, http://dx.doi.org/10.1016/j.jpowsour.2018.01.004.

[38] J. Cao, D. Harrold, Z. Fan, T. Morstyn, D. Healey, K. Li, Deep reinforcement learning-based energy storage arbitrage with accurate lithium-ion battery degradation model, IEEE Trans. Smart Grid 11 (5) (2020) 4513–4521, http://dx.doi.org/10.1109/TSG.2020.2986333.

[39] Z. Yang, K. Li, A. Foley, Computational scheduling methods for integrating plug-in electric vehicles with power systems: A review, Renew. Sustain. Energy Rev. 51 (2015) 396–416, http://dx.doi.org/10.1016/j.rser.2015.06.007.

[40] A. Väyrynen, J. Salminen, Lithium ion battery production, J. Chem. Thermodyn. 46 (2012) 80–85, http://dx.doi.org/10.1016/j.jct.2011.09.005.

[41] C.R. Birkl, M.R. Roberts, E. McTurk, P.G. Bruce, D.A. Howey, Degradation diagnostics for lithium ion cells, J. Power Sources 341 (2017) 373–386, http://dx.doi.org/10.1016/j.jpowsour.2016.12.011.

[42] Y. Chu, Y. Shen, F. Guo, X. Zhao, Q. Dong, Q. Zhang, W. Li, H. Chen, Z. Luo, L. Chen, Advanced characterizations of solid electrolyte interphases in lithium-ion batteries, Electrochem. Energy Rev. 3 (1) (2020) 187–219, http://dx.doi.org/10.1007/s41918-019-00058-y.

[43] C. von Lüders, J. Keil, M. Webersberger, A. Jossen, Modeling of lithium plating and lithium stripping in lithium-ion batteries, J. Power Sources 414 (2019) 41–47, http://dx.doi.org/10.1016/j.jpowsour.2018.12.084.

[44] S. Hein, T. Danner, A. Latz, An electrochemical model of lithium plating and stripping in lithium ion batteries, ACS Appl. Energy Mater. 3 (9) (2020) 8519–8531, http://dx.doi.org/10.1021/acsaem.0c01155.

[45] Y. Chen, Y. Kang, Y. Zhao, L. Wang, J. Liu, Y. Li, Z. Liang, X. He, X. Li, N. Tavajohi, B. Li, A review of lithium-ion battery safety concerns: The issues, strategies, and testing standards, J. Energy Chem. 59 (2021) 83–99, http://dx.doi.org/10.1016/j.jechem.2020.10.017.

[46] L. Guo, D.B. Thornton, M.A. Koronfel, I.E.L. Stephens, M.P. Ryan, Degradation in lithium ion battery current collectors, J. Phys.: Energy 3 (3) (2021) 032015, http://dx.doi.org/10.1088/2515-7655/ac0c04.

[47] R. Xiong, Y. Pan, W. Shen, H. Li, F. Sun, Lithium-ion battery aging mechanisms and diagnosis method for automotive applications: Recent advances and perspectives, Renew. Sustain. Energy Rev. 131 (2020) 110048, http://dx.doi.org/10.1016/j.rser.2020.110048.

[48] S.-T. Myung, F. Maglia, K.-J. Park, C.S. Yoon, P. Lamp, S.-J. Kim, Y.-K. Sun, Nickel-rich layered cathode materials for automotive lithium-ion batteries: Achievements and perspectives, ACS Energy Lett. 2 (1) (2017) 196–223, http://dx.doi.org/10.1021/acsenergylett.6b00594.

[49] Y. Preger, H.M. Barkholtz, A. Fresquez, D.L. Campbell, B.W. Juba, J. Romàn-Kustas, S.R. Ferreira, B. Chalamala, Degradation of commercial lithium-ion cells as a function of chemistry and cycling conditions, J. Electrochem. Soc. 167 (2020) 120532, http://dx.doi.org/10.1149/1945-7111/abae37.

[50] E. Cabrera-Castillo, F. Niedermeier, A. Jossen, Calculation of the state of safety (SOS) for lithium ion batteries, J. Power Sources 324 (2016) 509–520, http://dx.doi.org/10.1016/j.jpowsour.2016.05.068.

[51] D. Ouyang, M. Chen, J. Liu, R. Wei, J. Weng, J. Wang, Investigation of a commercial lithium-ion battery under overcharge/over-discharge failure conditions, RSC Adv. 8 (58) (2018) 33414–33424, http://dx.doi.org/10.1039/C8RA05564E.

[52] P. Keil, S.F. Schuster, J. Wilhelm, J. Travi, A. Hauser, R.C. Karl, A. Jossen, Calendar aging of lithium-ion batteries: I. Impact of the graphie anode on capacity fade, J. Electrochem. Soc. 163 (9) (2016) A1872–A1880, http://dx.doi.org/10.1149/2.0411609jes.

[53] T. Waldmann, M. Wilka, M. Kasper, M. Fleischhammer, M. Wohlfahrt-Mehrens, Temperature dependent ageing mechanisms in lithium-ion batteries – A post-mortem study, J. Power Sources 262 (2014) 129–135, http://dx.doi.org/10.1016/j.jpowsour.2014.03.112.

[54] M. Schimpe, M.E.v. Kuepach, M. Naumann, H. Hesse, K. Smith, A. Jossen, Comprehensive modeling of temperature-dependent degradation mechanisms in lithium iron phosphate batteries, J. Electrochem. Soc. 165 (2) (2018) A181–A193, http://dx.doi.org/10.1149/2.1181714jes.

[55] J. Wang, W. Huang, A. Pei, Y. Li, F. Shi, X. Yu, Y. Cui, Improving cyclability of Li metal batteries at elevated temperatures and its origin revealed by cryo-electron microscopy, Nature Energy 4 (8) (2019) 664–670, http://dx.doi.org/10.1038/s41560-019-0413-3.

[56] P.M. Attia, W.C. Chueh, S.J. Harris, Revisiting the t0.5 dependence of SEI growth, J. Electrochem. Soc. 167 (9) (2020) 090535, http://dx.doi.org/10.1149/1945-7111/ab8ce4.

[57] S. Barcellona, L. Piegari, Effect of current on cycle aging of lithium ion batteries, J. Energy Storage 29 (2020) 101310, http://dx.doi.org/10.1016/j.est.2020.101310.

[58] A. Tomaszewska, Z. Chu, X. Feng, S. O'Kane, X. Liu, J. Chen, C. Ji, E. Endler, R. Li, L. Liu, Y. Li, S. Zheng, S. Vetterlein, M. Gao, J. Du, M. Parkes, M. Ouyang, M. Marinescu, G. Offer, B. Wu, Lithium-ion battery fast charging: A review, ETransportation 1 (15) (2019) 100011, http://dx.doi.org/10.1016/j.etran.2019.100011.

[59] S. Gantenbein, M. Schönleber, M. Weiss, E. Ivers-Tiffée, Capacity fade in lithium-ion batteries and cyclic aging over various state-of-charge ranges, Sustainability 11 (23) (2019) 6697, http://dx.doi.org/10.3390/su11236697.

[60] S. Schweidler, L. de Biasi, A. Schiele, P. Hartmann, T. Brezesinski, J. Janek, Volume changes of graphite anodes revisited: A combined operando X-ray diffraction and in situ pressure analysis study, J. Phys. Chem. C 122 (16) (2018) 8829–8835, http://dx.doi.org/10.1021/acs.jpcc.8b01873.

[61] R.D. Deshpande, K. Uddin, Physics inspired model for estimating 'cycles to failure' as a function of depth of discharge for lithium ion batteries, J. Energy Storage 33 (2) (2021) 101932, http://dx.doi.org/10.1016/j.est.2020.101932.

[62] M. Ecker, N. Nieto, S. Käbitz, J. Schmalstieg, H. Blanke, A. Warnecke, D.U. Sauer, Calendar and cycle life study of Li(NiMnCo)O2-based 18650 lithium-ion batteries, J. Power Sources 248 (9) (2014) 839–851, http://dx.doi.org/10.1016/j.jpowsour.2013.09.143.

[63] F.B. Spingler, M. Naumann, A. Jossen, Capacity recovery effect in commercial LiFePO4 / graphite cells, J. Electrochem. Soc. 167 (4) (2020) 040526, http://dx.doi.org/10.1149/1945-7111/ab7900.

[64] D. Juarez-Robles, J.A. Jeevarajan, P.P. Mukherjee, Degradation-safety analytics in lithium-ion cells: Part I. Aging under charge/discharge cycling, J. Electrochem. Soc. 167 (16) (2020) 160510, http://dx.doi.org/10.1149/1945-7111/abc8c0.

[65] S. Bazlen, P. Heugel, O. von Kessel, W. Commerell, J. Tübke, Influence of charging protocols on the charging capability and aging of lithium-ion cells with silicon-containing anodes, J. Energy Storage 49 (23) (2022) 104044, http://dx.doi.org/10.1016/j.est.2022.104044.

[66] J. Park, W.A. Appiah, S. Byun, D. Jin, M.-H. Ryou, Y.M. Lee, Semi-empirical long-term cycle life model coupled with an electrolyte depletion function for large-format graphite/LiFePO 4 lithium-ion batteries, J. Power Sources 365 (2017) 257–265, http://dx.doi.org/10.1016/j.jpowsour.2017.08.094.

[67] A. Kwade, W. Haselrieder, R. Leithoff, A. Modlinger, F. Dietrich, K. Droeder, Current status and challenges for automotive battery production technologies, Nature Energy 3 (4) (2018) 290–300, http://dx.doi.org/10.1038/s41560-018-0130-3.

[68] S.J. An, J. Li, Z. Du, C. Daniel, D.L. Wood, Fast formation cycling for lithium ion batteries, J. Power Sources 342 (2017) 846–852, http://dx.doi.org/10.1016/j.jpowsour.2017.01.011.

[69] S.F. Schuster, T. Bach, E. Fleder, J. Müller, M. Brand, G. Sextl, A. Jossen, Nonlinear aging characteristics of lithium-ion cells under different operational conditions, J. Energy Storage 1 (2015) 44–53, http://dx.doi.org/10.1016/j.est.2015.05.003.

[70] X.-G. Yang, Y. Leng, G. Zhang, S. Ge, C.-Y. Wang, Modeling of lithium plating induced aging of lithium-ion batteries: Transition from linear to nonlinear aging, J. Power Sources 360 (2017) 28–40, http://dx.doi.org/10.1016/j.jpowsour.2017.05.110.

[71] D. Anseán, M. Dubarry, A. Devie, B.Y. Liaw, V.M. García, J.C. Viera, M. González, Operando lithium plating quantification and early detection of a commercial LiFePO4 cell cycled under dynamic driving schedule, J. Power Sources 356 (2) (2017) 36–46, http://dx.doi.org/10.1016/j.jpowsour.2017.04.072.

[72] C. Kupper, B. Weißhar, S. Rißmann, W.G. Bessler, End-of-life prediction of a lithium-ion battery cell based on mechanistic aging models of the graphite electrode, J. Electrochem. Soc. 165 (14) (2018) A3468–A3480, http://dx.doi.org/10.1149/2.0941814jes.

[73] P.M. Attia, A. Bills, F. Brosa Planella, P. Dechent, G. dos Reis, M. Dubarry, P. Gasper, R. Gilchrist, S. Greenbank, D. Howey, O. Liu, E. Khoo, Y. Preger, A. Soni, S. Sripad, A.G. Stefanopoulou, V. Sulzer, Review—"knees" in lithium-ion battery aging trajectories, Journal of the Electrochemical Society 169 (6) (2022) 060517, http://dx.doi.org/10.1149/1945-7111/ac6d13.

[74] M. Johnen, S. Pitzen, U. Kamps, M. Kateri, P. Dechent, D.U. Sauer, Modeling long-term capacity degradation of lithium-ion batteries, J. Energy Storage 34 (9) (2021) 102011, http://dx.doi.org/10.1016/j.est.2020.102011.

[75] G. He, R. Ciez, P. Moutis, S. Kar, J.F. Whitacre, The economic end of life of electrochemical energy storage, Appl. Energy 273 (2020) 115151, http://dx.doi.org/10.1016/j.apenergy.2020.115151.

[76] P. Fermín-Cueto, E. McTurk, M. Allerhand, E. Medina-Lopez, M.F. Anjos, J. Sylvester, G. dos Reis, Identification and machine learning prediction of knee-point and knee-onset in capacity degradation curves of lithium-ion cells, Energy AI 1 (5) (2020) 100006, http://dx.doi.org/10.1016/j.egyai.2020.100006.

[77] D. Ren, H. Hsu, R. Li, X. Feng, D. Guo, X. Han, L. Lu, X. He, S. Gao, J. Hou, Y. Li, Y. Wang, M. Ouyang, A comparative investigation of aging effects on thermal runaway behavior of lithium-ion batteries, ETransportation 2 (2019) 100034, http://dx.doi.org/10.1016/j.etran.2019.100034.

[78] Y. Li, X. Feng, D. Ren, M. Ouyang, L. Lu, X. Han, Thermal runaway triggered by plated lithium on the anode after fast charging, ACS Appl. Mater. Interfaces 11 (50) (2019) 46839–46850, http://dx.doi.org/10.1021/acsami.9b16589.

[79] L. Feng, L. Jiang, J. Liu, Z. Wang, Z. Wei, Q. Wang, Dynamic overcharge investigations of lithium ion batteries with different state of health, J. Power Sources 507 (6) (2021) 230262, http://dx.doi.org/10.1016/j.jpowsour.2021.230262.

[80] G. He, Q. Chen, C. Kang, P. Pinson, Q. Xia, Optimal bidding strategy of battery storage in power markets considering performance-based regulation and battery cycle life, IEEE Trans. Smart Grid 7 (5) (2016) 2359–2367, http://dx.doi.org/10.1109/TSG.2015.2424314.

[81] M. Kazemi, H. Zareipour, Long-term scheduling of battery storage systems in energy and regulation markets considering battery's lifespan, IEEE Trans. Smart Grid 9 (6) (2018) 6840–6849, http://dx.doi.org/10.1109/TSG.2017.2724919.

[82] M.A. Hossain, H.R. Pota, S. Squartini, F. Zaman, J.M. Guerrero, Energy scheduling of community microgrid with battery cost using particle swarm optimisation, Appl. Energy 254 (9) (2019) 113723, http://dx.doi.org/10.1016/j.apenergy.2019.113723.

[83] Y. Shi, B. Xu, Y. Tan, D. Kirschen, B. Zhang, Optimal battery control under cycle aging mechanisms in pay for performance settings, IEEE Trans. Automat. Control 64 (6) (2019) 2324–2339, http://dx.doi.org/10.1109/TAC.2018.2867507.

[84] N. Padmanabhan, M. Ahmed, K. Bhattacharya, Battery energy storage systems in energy and reserve markets, IEEE Trans. Power Syst. 35 (1) (2020) 215–226, http://dx.doi.org/10.1109/TPWRS.2019.2936131.

[85] A. Maheshwari, N.G. Paterakis, M. Santarelli, M. Gibescu, Optimizing the operation of energy storage using a non-linear lithium-ion battery degradation model, Appl. Energy 261 (4) (2020) 114360, http://dx.doi.org/10.1016/j.apenergy.2019.114360.

[86] C. Guenther, B. Schott, W. Hennings, P. Waldowski, M.A. Danzer, Model-based investigation of electric vehicle battery aging by means of vehicle-to-grid scenario simulations, J. Power Sources 239 (2013) 604–610, http://dx.doi.org/10.1016/j.jpowsour.2013.02.041.

[87] B. Xu, A. Oudalov, A. Ulbig, G. Andersson, D.S. Kirschen, Modeling of lithium-ion battery degradation for cell life assessment, IEEE Trans. Smart Grid 9 (2) (2018) 1131–1140, http://dx.doi.org/10.1109/TSG.2016.2578950.

[88] P. Gasper, K. Gering, E. Dufek, K. Smith, Challenging practices of algebraic battery life models through statistical validation and model identification via machine-learning, J. Electrochem. Soc. 168 (2021) 020502, http://dx.doi.org/10.1149/1945-7111/abdde1.

[89] M. Broussely, S. Herreyre, P. Biensan, P. Kasztejna, K. Nechev, R.J. Staniewicz, Aging mechanism in Li ion cells and calendar life predictions, J. Power Sources 97–98 (2001) 13–21, http://dx.doi.org/10.1016/S0378-7753(01)00722-4.

[90] S. Grolleau, A. Delaille, H. Gualous, P. Gyan, R. Revel, J. Bernard, E. Redondo-Iglesias, J. Peter, Calendar aging of commercial graphite/LiFePO4 cell – predicting capacity fade under time dependent storage conditions, J. Power Sources 255 (2014) 450–458, http://dx.doi.org/10.1016/j.jpowsour.2013.11.098.

[91] S. Khaleghi Rahimian, M.M. Forouzan, S. Han, Y. Tang, A generalized physics-based calendar life model for Li-ion cells, Electrochim. Acta 348 (2020) 136343, http://dx.doi.org/10.1016/j.electacta.2020.136343.

[92] J. Wang, P. Liu, J. Hicks-Garner, E. Sherman, S. Soukiazian, M. Verbrugge, H. Tataria, J. Musser, P. Finamore, Cycle-life model for graphite-LiFePO4 cells, J. Power Sources 196 (8) (2011) 3942–3948, http://dx.doi.org/10.1016/j.jpowsour.2010.11.134.

[93] K.J. Laidler, The development of the arrhenius equation, J. Chem. Educ. 61 (1984) 494–498, http://dx.doi.org/10.1021/ed061p494.

[94] A. Maheshwari, M. Heck, M. Santarelli, Cycle aging studies of lithium nickel manganese cobalt oxide-based batteries using electrochemical impedance spectroscopy, Electrochim. Acta 273 (1) (2018) 335–348, http://dx.doi.org/10.1016/j.electacta.2018.04.045.

[95] K. Smith, A. Saxon, M. Keyser, B. Lundstrom, Z. Cao, A. Roc, Life prediction model for grid-connected Li-ion battery energy storage system, in: 2017 American Control Conference (ACC), IEEE, 2017, pp. 4062–4068, http://dx.doi.org/10.23919/ACC.2017.7963578.

[96] X. Jin, A. Vora, V. Hoshing, T. Saha, G. Shaver, O. Wasynczuk, S. Varigonda, Applicability of available Li-ion battery degradation models for system and control algorithm design, Control Eng. Pract. 71 (8) (2018) 1–9, http://dx.doi.org/10.1016/j.conengprac.2017.10.002.

[97] J. Li, K. Adewuyi, N. Lotfi, R.G. Landers, J. Park, A single particle model with chemical/mechanical degradation physics for lithium ion battery state of health (SOH) estimation, Appl. Energy 212 (4) (2018) 1178–1190, http://dx.doi.org/10.1016/j.apenergy.2018.01.011.

[98] G. Ning, B.N. Popov, Cycle life modeling of lithium-ion batteries, J. Electrochem. Soc. 151 (10) (2004) A1584–A1591, http://dx.doi.org/10.1149/1.1787631.

[99] M.B. Pinson, M.Z. Bazant, Theory of SEI formation in rechargeable batteries: Capacity fade, accelerated aging and lifetime prediction, J. Electrochem. Soc. 160 (2) (2013) A243–A250, http://dx.doi.org/10.1149/2.044302jes.

[100] M. Doyle, T.F. Fuller, J. Newman, Modeling of galvanostatic charge and discharge of the lithium/polymer/insertion cell, J. Electrochem. Soc. 140 (1993) 1526–1533, http://dx.doi.org/10.1149/1.2221597.

[101] M. Doyle, J. Newman, Modeling the performance of rechargeable lithium-based cells: design correlations for limiting cases, J. Power Sources (1995) 45–51, http://dx.doi.org/10.1016/0378-7753(94)02038-5.

[102] T.R. Ashwin, Y.M. Chung, J. Wang, Capacity fade modelling of lithium-ion battery under cyclic loading conditions, J. Power Sources 328 (2016) 586–598, http://dx.doi.org/10.1016/j.jpowsour.2016.08.054.

[103] J. Keil, A. Jossen, Electrochemical modeling of linear and nonlinear aging of lithium-ion cells, J. Electrochem. Soc. 167 (11) (2020) 110535, http://dx.doi.org/10.1149/1945-7111/aba44f.

[104] C. Hu, H. Ye, G. Jain, C. Schmidt, Remaining useful life assessment of lithium-ion batteries in implantable medical devices, J. Power Sources 375 (2018) 118–130, http://dx.doi.org/10.1016/j.jpowsour.2017.11.056.

[105] M. Lucu, E. Martinez-Laserna, I. Gandiaga, K. Liu, H. Camblong, W.D. Widanage, J. Marco, Data-driven nonparametric Li-ion battery ageing model aiming at learning from real operation data - part B: Cycling operation, J. Energy Storage 30 (3) (2020) 101410, http://dx.doi.org/10.1016/j.est.2020.101410.

[106] Kristen A. Severson, Peter M. Attia, Norman Jin, Nicholas Perkins, Benben Jiang, Zi Yang, Michael H. Chen, Muratahan Aykol, Patrick K. Herring, Dimitrios Fraggedakis, Martin Z. Bazant, Stephen J. Harris, William C. Chueh, Richard D. Braatz, Data-driven prediction of battery cycle life before capacity degradation, Nature Energy 4 (2019) 383–391, http://dx.doi.org/10.1038/s41560-019-0356-8.

[107] Z. Deng, X. Lin, J. Cai, X. Hu, Battery health estimation with degradation pattern recognition and transfer learning, J. Power Sources 525 (2022) 231027, http://dx.doi.org/10.1016/j.jpowsour.2022.231027.

[108] W. Li, N. Sengupta, P. Dechent, D. Howey, A. Annaswamy, D.U. Sauer, One-shot battery degradation trajectory prediction with deep learning, J. Power Sources 506 (1) (2021) 230024, http://dx.doi.org/10.1016/j.jpowsour.2021.230024.

[109] X. Tang, K. Liu, X. Wang, F. Gao, J. Macro, W.D. Widanage, Model migration neural network for predicting battery aging trajectories, IEEE Trans. Transp. Electrif. 6 (2) (2020) 363–374, http://dx.doi.org/10.1109/TTE.2020.2979547.

[110] M. Dubarry, A. Devie, K. Stein, M. Tun, M. Matsuura, R. Rocheleau, Battery energy storage system battery durability and reliability under electric utility grid operations: Analysis of 3 years of real usage, J. Power Sources 338 (2) (2017) 65–73, http://dx.doi.org/10.1016/j.jpowsour.2016.11.034.

[111] T. Raj, A.A. Wang, C.W. Monroe, D.A. Howey, Investigation of path–dependent degradation in lithium–Ion batteries**, Batter. Supercaps 3 (12) (2020) 1377–1385, http://dx.doi.org/10.1002/batt.202000160.

[112] G. Baure, A. Devie, M. Dubarry, Battery durability and reliability under electric utility grid operations: Path dependence of battery degradation, J. Electrochem. Soc. (2019) A1991–A2001.

[113] B. Xu, J. Zhao, T. Zheng, E. Litvinov, D.S. Kirschen, Factoring the cycle aging cost of batteries participating in electricity markets, IEEE Trans. Power Syst. 33 (2) (2018) 2248–2259, http://dx.doi.org/10.1109/TPWRS.2017.2733339.

[114] V. Muenzel, J. de Hoog, M. Brazil, A. Vishwanath, S. Kalyanaraman, A multi-factor battery cycle life prediction methodology for optimal battery management, in: S. Kalyanaraman, D.P. Seetharam, R. Shorey, S. Ramchurn, M. Srivastava (Eds.), Proceedings of the 2015 ACM Sixth International Conference on Future Energy Systems, ACM, New York, NY, USA, 2015, pp. 57–66, http://dx.doi.org/10.1145/2768510.2768532.

[115] A. Nuhic, T. Terzimehic, T. Soczka-Guth, M. Buchholz, K. Dietmayer, Health diagnosis and remaining useful life prognostics of lithium-ion batteries using data-driven methods, J. Power Sources 239 (3) (2013) 680–688, http://dx.doi.org/10.1016/j.jpowsour.2012.11.146.

[116] Y. Shi, B. Xu, Di Wang, B. Zhang, Using battery storage for peak shaving and frequency regulation: Joint optimization for superlinear gains, IEEE Trans. Power Syst. 33 (3) (2018) 2882–2894, http://dx.doi.org/10.1109/TPWRS.2017.2749512.

[117] G. Suri, S. Onori, A control-oriented cycle-life model for hybrid electric vehicle lithium-ion batteries, Energy 96 (2) (2016) 644–653, http://dx.doi.org/10.1016/j.energy.2015.11.075.

[118] H. Hesse, V. Kumtepeli, M. Schimpe, J. Reniers, D. Howey, A. Tripathi, Y. Wang, A. Jossen, Ageing and efficiency aware battery dispatch for arbitrage markets using mixed integer linear programming, Energies 12 (6) (2019) 999, http://dx.doi.org/10.3390/en12060999.

[119] G. Angenendt, S. Zurmühlen, H. Axelsen, D.U. Sauer, Comparison of different operation strategies for PV battery home storage systems including forecast-based operation strategies, Appl. Energy 229 (1) (2018) 884–899, http://dx.doi.org/10.1016/j.apenergy.2018.08.058.

[120] S. Li, J. Li, C. Su, Q. Yang, Optimization of bi-directional V2G behavior with active battery anti-aging scheduling, IEEE Access 8 (2020) 11186–11196, http://dx.doi.org/10.1109/ACCESS.2020.2964699.

[121] Mónica Aguado, Elixabete Ayerbe, Cristina Azcárate, Rosa Blanco, Raquel Garde, Fermín Mallor, David M. Rivas, Economical assessment of a wind–hydrogen energy system using WindHyGen® software, Int. J. Hydrogen Energy 34 (7) (2009) 2845–2854, http://dx.doi.org/10.1016/j.ijhydene.2008.12.098.

[122] T. Weitzel, M. Schneider, C.H. Glock, F. Löber, S. Rinderknecht, Operating a storage-augmented hybrid microgrid considering battery aging costs, J. Cleaner Prod. 188 (7) (2018) 638–654, http://dx.doi.org/10.1016/j.jclepro.2018.03.296.

[123] W.B. Powell, Approximate Dynamic Programming: Solving the Curses of Dimensionality, Vol. 703, John Wiley & Sons, 2011.

[124] F. Wankmüller, P.R. Thimmapuram, K.G. Gallagher, A. Botterud, Impact of battery degradation on energy arbitrage revenue of grid-level energy storage, J. Energy Storage 10 (2017) 56–66, http://dx.doi.org/10.1016/j.est.2016.12.004.

[125] A. Perez, R. Moreno, R. Moreira, M. Orchard, G. Strbac, Effect of battery degradation on multi-service portfolios of energy storage, IEEE Trans. Sustain. Energy 7 (4) (2016) 1718–1729, http://dx.doi.org/10.1109/TSTE.2016.2589943.

[126] G. Cardoso, T. Brouhard, N. DeForest, D. Wang, M. Heleno, L. Kotzur, Battery aging in multi-energy microgrid design using mixed integer linear programming, Appl. Energy 231 (2018) 1059–1069, http://dx.doi.org/10.1016/j.apenergy.2018.09.185.

[127] J. Li, M.A. Danzer, Optimal charge control strategies for stationary photovoltaic battery systems, J. Power Sources 258 (2014) 365–373, http://dx.doi.org/10.1016/j.jpowsour.2014.02.066.

[128] E. Kruger, Q.T. Tran, Minimal aging operating strategies for battery energy storage systems in photovoltaic applications, in: 2016 IEEE PES Innovative Smart Grid Technologies Conference Europe (ISGT-Europe), IEEE, 2016, pp. 1–6, http://dx.doi.org/10.1109/ISGTEurope.2016.7856325.

[129] W.-W. Kim, J.-S. Shin, S.-Y. Kim, J.-O. Kim, Operation scheduling for an energy storage system considering reliability and aging, Energy 141 (2017) 389–397, http://dx.doi.org/10.1016/j.energy.2017.09.091.

[130] K. Abdulla, J. de Hoog, V. Muenzel, F. Suits, K. Steer, A. Wirth, S. Halgamuge, Optimal operation of energy storage systems considering forecasts and battery degradation, IEEE Trans. Smart Grid 9 (3) (2016) 2086–2096, http://dx.doi.org/10.1109/TSG.2016.2606490.

[131] X. Jin, A. Vora, V. Hoshing, T. Saha, G. Shaver, R.E. García, O. Wasynczuk, S. Varigonda, Physically-based reduced-order capacity loss model for graphite anodes in Li-ion battery cells, J. Power Sources 342 (9) (2017) 750–761, http://dx.doi.org/10.1016/j.jpowsour.2016.12.099.

[132] M.A. Ortega-Vazquez, Optimal scheduling of electric vehicle charging and vehicle–to–grid services at household level including battery degradation and price uncertainty, IET Gener. Transm. Distrib. 8 (6) (2014) 1007–1016, http://dx.doi.org/10.1049/iet-gtd.2013.0624.

[133] X. Qing, X. Lin, Y. Wang, M. Pedram, D. Shin, N. Chang, State of health aware charge management in hybrid electrical energy storage systems, in: 2012 Design, Automation & Test in Europe Conference & Exhibition (DATE), IEEE, 2012, pp. 1060–1065, http://dx.doi.org/10.1109/DATE.2012.6176652.

[134] M.F. Zia, E. Elbouchikhi, M. Benbouzid, Optimal operational planning of scalable DC microgrid with demand response, islanding, and battery degradation cost considerations, Appl. Energy 237 (2019) 695–707, http://dx.doi.org/10.1016/j.apenergy.2019.01.040.

[135] D. Magnor, Globale Optimierung Netzgekoppelter PV-Batteriesysteme Unter Besonderer Berücksichtigung der Batteriealterung (Ph.D. thesis), 2017, http://dx.doi.org/10.18154/RWTH-2017-06592.

[136] B.E. Olivares, M.A. Cerda Munoz, M.E. Orchard, J.F. Silva, Particle-filtering-based prognosis framework for energy storage devices with a statistical characterization of state-of-health regeneration phenomena, IEEE Trans. Instrum. Meas. 62 (2) (2013) 364–376, http://dx.doi.org/10.1109/TIM.2012.2215142.

[137] D. Wang, J. Coignard, T. Zeng, C. Zhang, S. Saxena, Quantifying electric vehicle battery degradation from driving vs. vehicle-to-grid services, J. Power Sources 332 (2016) 193–203, http://dx.doi.org/10.1016/j.jpowsour.2016.09.116.

[138] S.B. Peterson, J. Apt, J.F. Whitacre, Lithium-ion battery cell degradation resulting from realistic vehicle and vehicle-to-grid utilization, J. Power Sources 195 (8) (2010) 2385–2392, http://dx.doi.org/10.1016/j.jpowsour.2009.10.010.

[139] S. Watanabe, M. Kinoshita, T. Hosokawa, K. Morigaki, K. Nakura, Capacity fade of LiAlyNi1−x−yCoxO2 cathode for lithium-ion batteries during accelerated calendar and cycle life tests (surface analysis of LiAlyNi1−x−yCoxO2 cathode after cycle tests in restricted depth of discharge ranges), J. Power Sources 258 (2014) 210–217, http://dx.doi.org/10.1016/j.jpowsour.2014.02.018.

[140] G. Notton, V. Lazarov, L. Stoyanov, Optimal sizing of a grid-connected PV system for various PV module technologies and inclinations, inverter efficiency characteristics and locations, Renew. Energy 35 (2) (2010) 541–554, http://dx.doi.org/10.1016/j.renene.2009.07.013.

[141] 50Hertz Transmission GmbH, Archiv netzfrequenz (in German): Daten der ENTSO-E netzfrequenz, 2019, URL https://www.50hertz.com/de/Transparenz/Kennzahlen/Regelenergie/ArchivNetzfrequenz.

[142] T. Tjaden, J. Bergner, J. Weniger, V. Quaschning, Repräsentative elektrische lastprofile für wohngebäude in deutschland auf 1-sekündiger datenbasis (in German), 2015, URL https://pvspeicher.htw-berlin.de/veroeffentlichungen/daten/.

[143] M. Möller, D. Kucevic, N. Collath, A. Parlikar, P. Dotzauer, B. Tepe, S. Englberger, A. Jossen, H. Hesse, SimSES: A holistic simulation framework for modeling and analyzing stationary energy storage systems, J. Energy Storage 49 (11) (2022) 103743, http://dx.doi.org/10.1016/j.est.2021.103743.

[144] N. Collath, B. Tepe, S. Englberger, A. Jossen, H. Holger, Battery degradation in BESS use-cases with varying degradation models and stress factor assumptions, 2022, http://dx.doi.org/10.14459/2022mp1652796.